 Bull. Chem. Soc. Jpn., 74, 2223–2253 (2001)

Accounts

Calorimetric Investigations of Phase Transitions Occurring in Molecule-Based Materials in Which Electrons Are Directly Involved#

Michio Sorai

Research Center for Molecular Thermodynamics, Graduate School of Science, Osaka University, Toyonaka, Osaka 560-0043

(Received June 20, 2001)

New types of phase transitions occurring in molecule-based materials have recently drawn great attention, in which electrons are directly involved. In this paper are given calorimetric investigations aimed at the elucidation of the mechanisms governing such phase transitions as (i) spin crossover phenomena occurring between high- and low-spin states in transition-metal complexes, (ii) intramolecular electron transfers in mixed-valence complexes, (iii) neutral-to-ionic transitions due to charge transfer mechanism, and (iv) thermochromic phenomena due to a change in coordination geometry. Since a change in the electronic state is strongly coupled with a change in the lattice, it turns out that the transition mechanisms always include interplays with various molecular motions in the lattice. In all these systems, a large change in the electronic energy is compensated by the entropy term due to these molecular motions.

Phase transitions occurring in condensed states manifest themselves as concerted effects of molecular structure, intermolecular interactions, and molecular motions. Phase transitions are, therefore, very efficient probes for the better understanding of materials. Hitherto well-known phase transitions include the order-disorder type and the displacement type.[1] The order-disorder type phase transition involves a change in the orientational alignment of molecular- or spin-axes. On the other hand, the displacement-type phase transition concerns the displacement of atomic or molecular positions. Since intramolecular electronic energy is much greater than intermolecular potential energy, the change in the electronic energy of a molecule is negligibly small when phase transitions take place. In other words, the molecular structure remains unchanged through phase transitions.

However, new types of phase transitions occurring in molecule-based materials have recently drawn great attention. In such phase transitions, electrons are directly involved, since a change in the electronic state is strongly coupled with a change in the lattice. As summarized in Table 1, representatives of such exotic phase transitions are (i) spin crossover phenomena occurring between high and low spin states in transition-metal complexes, (ii) intramolecular electron transfers in mixed-valence complexes, (iii) neutral-to-ionic transitions due to charge transfer mechanism, (iv) thermochromic phenomena due to a change in coordination geometry, and (v) metal-to-insulator transitions known as the Peierls transitions.

Contribution No.46 from the Research Center for Molecular Thermodynamics.

In this paper, calorimetric investigations aimed at the elucidation of the mechanisms governing each phase transition in molecule-based materials will be described.

1. Heat-Capacity Calorimetry

Heat capacity is very sensitive to a change in the degree of short-range or long-range order in the condensed states of matter.[2–4] Consequently, heat-capacity calorimetry is the most reliable experimental tool to detect the existence of phase transitions originating in the onset of a long-range ordering. Heat capacity is usually measured under constant pressure and designated as C_p. It is defined as "the enthalpy H required for raising the temperature of one mole of a given substance by 1 K". From this definition, $C_p = (\partial H/\partial T)_p$, enthalpy increment is determined by integration of C_p with respect to temperature T:

$$H = \int C_p \, \mathrm{d}T$$

Since C_p is alternatively defined as $C_p = T\,(\partial S/\partial T)_p$, entropy S is also obtainable by integration of C_p with respect to $\ln T$:

$$S = \int C_p \, \mathrm{d} \ln T$$

Now that both the enthalpy and entropy are derived from C_p measurements, one can estimate the Gibbs energy as $G = H - TS$. Heat capacity is a very efficient physical quantity, in that three fundamental thermodynamic quantities (H, S and G) can be simultaneously determined solely from C_p measurements.

The merit of calorimetry, though also the shortcoming in

Table 1. Characteristic Aspects of Phase Transitions in Which Electrons Are Directly Involved

	Phase transition	Phenomenon
(1)	Spin crossover	Low spin ⇄ High spin
(2)	Intramolecular electron transfer in mixed-valence complexes	Valence trapped ⇄ Valence detrapped
(3)	Thermochromism	Change in ligand geometry and thus the change in the electronic state
(4)	Charge transfer	Ionic ⇄ Neutral
(5)	Peierls transition	Insulator ⇄ Metal

some cases, is that contributions from all the degrees of freedom are principally involved in each experimental heat capacity. Therefore, for discussion of the nature of a phase transition, the contribution from each relevant degree of freedom must be accurately separated from the observed heat capacity. The onset of the long-range order appears as a sharp C_p peak at the phase transition temperature, while the short-range order is detected as heat capacity anomaly ΔC_p beyond a normal (or lattice) heat capacity. The excess enthalpy ΔH and entropy ΔS arising from the phase transition and/or the heat capacity anomalies can be determined by integration of ΔC_p with respect to T and ln T, respectively. Based on these quantities, one can gain an insight into the mechanism of the phase transition.

Although entropy is a physical quantity characteristic of the macroscopic aspects of a system, the Boltzmann principle interrelates such macroscopic entropy with the number of thermally accessible microscopic states:

$$S = k N_A \ln W = R \ln W,$$

where k and N_A are the Boltzmann and Avogadro constants, R the gas constant, and W stands for the number of microscopic states. If one applies this principle to the transition entropy, the following relationship is easily derived, because ΔS is the entropy difference between the high- and low-temperature phases: $\Delta S = R \ln (W_H/W_L)$, where W_H and W_L mean the number of microscopic states in the high- and low-temperature phases, respectively. In many cases, the low-temperature phase corresponds to an ordered state and hence $W_L = 1$. Therefore, when a phase transition is concerned with an order–disorder type, one can determine the number of microscopic states W_H in the high-temperature phase on the basis of the experimental ΔS value.

We constructed sophisticated heat-capacity calorimeters with very high accuracy and precision: (i) an adiabatic calorimeter for the 1–20 K range,[5] (ii) a ^{3}He calorimeter for the 0.4–20 K range,[6] (iii) a very-low temperature calorimeter with a (^{3}He + ^{4}He) dilution refrigerator for the 0.04–20 K range,[7] (iv) an automated adiabatic calorimeter for the 13–393 K range,[8] (v) an automated adiabatic calorimeter for the 13–530 K range,[9] and (vi) a chopped-light ac calorimeter with highly stable thermal condition.[10] By use of these calorimeters, the present author and his collaborators have measured heat capacities of various kinds of materials and have revealed many essential aspects inherent in the novel phase transitions.

2. Change in the Electronic State due to Molecular Motion in the Organometallic Compound $[Co_3(C_5H_5)_3S_2]$

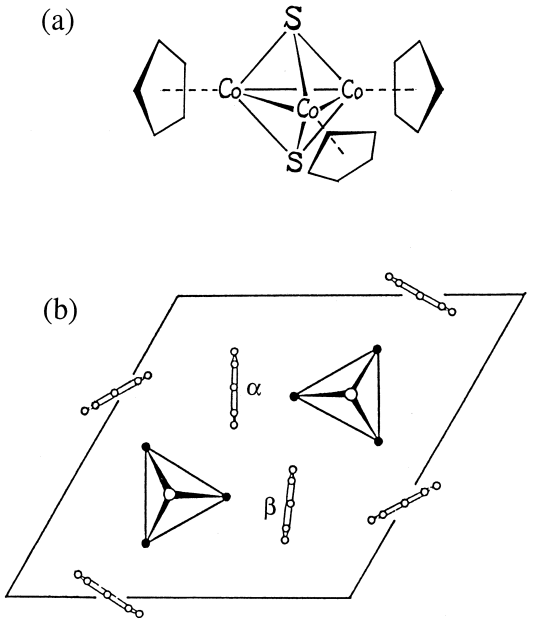

Fig. 1. (a) Molecular configuration and (b) projection on the (001) plane of the crystal structure of the organometallic compound $[Co_3(C_5H_5)_3S_2]$ (Ref. 15).

Our motivation for the investigations of phase transitions, in which electrons are directly involved, originates in a calorimetric study[11] done in 1971 on an organometallic compound, tris-(π-cyclopentadienylcobalt) disulfide $[Co_3(C_5H_5)_3S_2]$ (see Fig. 1a). Solid state magnetic susceptibility measurements[12–14] showed that this compound exhibits Curie–Weiss behavior from 340 to 196 K, where an abrupt discontinuity occurs such that around 170 K the magnetic susceptibility drops sharply to approximately half of its maximum value. We measured its heat capacity over a wide temperature region by adiabatic calorimetry (see Fig. 2) and discovered a phase transition at 192.5 K with the transition entropy of 28.9 J K^{-1} mol^{-1}. On the basis of the complementary solid-state magnetic and thermal data, we elucidated that this phase transition must be associated with a cooperative coupling between a gear-like rotational motion of reorientating cyclopentadienyl rings and a change in the molecular electronic state which is dramatically altered by the reorientational motion of cyclopentadienyl rings.

The packing of cyclopentadienyl rings belonging to the adjacent molecules, which are indicated for example as α and β in Fig. 1b,[15] has a close resemblance to that in ferrocene crystal along the c-axis.[16] As in the case of ferrocene, we assumed that each cyclopentadienyl ring of $[Co_3(C_5H_5)_3S_2]$ can orient in two directions about the C_5-axis of the cyclopentadienyl ring in

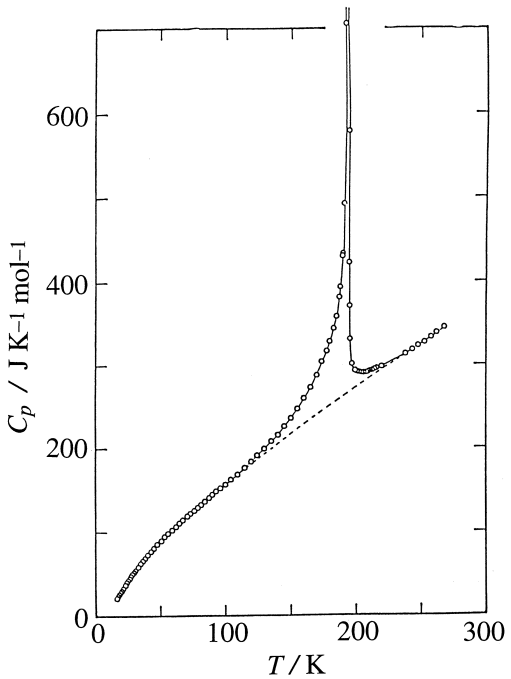

Fig. 2. Molar heat capacity of $[Co_3(C_5H_5)_3S_2]$. Broken curve indicates the normal heat capacity (Ref. 11).

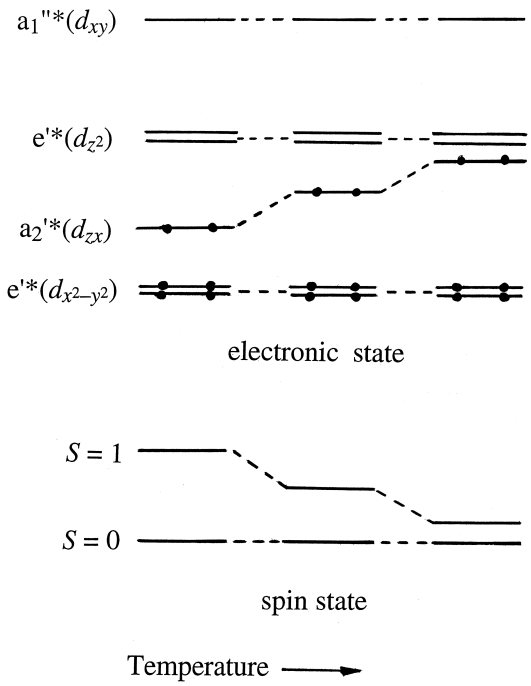

Fig. 3. Temperature dependence of the electronic states of $[Co_3(C_5H_5)_3S_2]$ (see the text for the meaning of the molecular orbital symbols) (Ref. 11).

the room temperature phase. We further assumed that the interaction between three rings belonging to the identical molecule would be negligible, as each ring is separated far from the other two by a large core of cobalt and sulfur atoms. On these assumptions, the number of energetically equivalent configurations attainable for one molecule may be eight ($= 2^3$) and thus the configurational entropy due to the order–disorder phenomenon of the cyclopentadieny rings amounts to R ln 8 ($= 17.28$ J K^{-1} mol^{-1}).

Sorai et al.[11] proposed that the magnetic behavior of this compound can only be explained by a level crossing of two close-lying MOs: a non-degenerate $a_2'^*(d_{zx})$ and a doubly degenerate $e'^*(d_{z^2})$ (under assumed D_{3h} symmetry). As we are interested in a relationship between the electronic state and the spin state, our discussion is confined to four antibonding orbitals concerning the 3d-orbitals of the cobalt atoms. For example, the d_{z^2} orbitals of three cobalt atoms combine to give doubly degenerate antibonding MOs, $e'^*(d_{z^2})$. The energy level $e'^*(d_{z^2})$ is nearly independent of temperature, as the orbital overlap between this and the π-orbitals of each cyclopentadienyl ring is not affected by the onset of the reorientational motion of the C_5H_5-ring. On the other hand, the $a_2'^*(d_{zx})$ is sensitive to the motional behavior of the ring. Therefore, it is reasonable to assume that the energy of $a_2'^*(d_{zx})$ orbital is destabilized and the energy-distance between this orbital and $e'^*(d_{z^2})$ orbital becomes narrower with increasing temperature. Although this new idea was crucially important, as Dahl et al.[17] pointed out, our proposed temperature-dependent energy scheme was unfortunately flawed by the assignment of an incorrect number of electrons (i.e., four instead of two) to the frontier $a_2'^*$ and e'^* MOs. Figure 3 demonstrates the corrected electronic scheme, in which the level-distance between the $a_2'^*$ and e'^* energy levels is actually diminished with increasing temperature: the $a_2'^*$ level locates lower and is doubly occupied at low temperatures (singlet spin state) while the e'^* levels are thermally accessible at high temperatures (triplet spin state). Frisch and Dahl[18] likewise rationalized the ^{1}H NMR singlet-triplet data in terms of the existence of temperature sensitive $a_2'^*$ level.

The unusually large entropy gain at this phase transition (28.9 J K^{-1} mol^{-1}) was well accounted for[11] in terms of a cooperative coupling (28.8 J K^{-1} mol^{-1}) between the magnetic contribution arising from the singlet to triplet excitation of electrons (modified Chesnut model:[19] R ln 4 = 11.53 J K^{-1} mol^{-1}) and the order–disorder configurational contribution (R ln 2^3 = 17.28 J K^{-1} mol^{-1}) due to gear-like reorientational motion of the cyclopentadienyl rings, each of which may take two orientations.

3. Spin Crossover Phenomena

Octahedral transition metal complexes having d^4, d^5, d^6, and d^7 electronic configurations can exist either in the high-spin or in the low-spin ground state depending on the ligand field strength (see Table 2). The spin state transition can occur between the two spin states when the field strength is close to the electron pairing energy. The possibility of this phenomenon was theoretically predicted in 1954 on the basis of the ligand field theory by Tanabe and Sugano,[20] while the first experimental evidence was reported for iron(II) complexes $[Fe^{II}(NCX)_2(phen)_2]$ (X = S or Se; phen = 1,10-phenanthroline) in 1967 by König and Madeja.[21] They gave a reasonable interpretation (as due to a spin crossover mechanism) for the unusual magnetic behaviors of these complexes reported first by Baker and Bobonich[22] in 1964. Since the spin crossover phenomenon is principally based on a change in the quantum state of the electron spin, many researchers believed that the dominant driving

Table 2. Ground Term and Spin Quantum Number Inherent in the High- and Low-Spin States of 3d Coordination Compound in the Octahedral Ligand Field (n: Number of 3d Electron)

n	Ion	High-spin state			Low-spin state		
4	Cr^{2+}, Mn^{3+}	$t_{2g}^3e_g^1$	^5E_g	$S = 2$	t_{2g}^4	$^3T_{1g}$	$S = 1$
5	Mn^{2+}, Fe^{3+}	$t_{2g}^3e_g^2$	$^6A_{1g}$	$S = 5/2$	t_{2g}^5	$^2T_{2g}$	$S = 1/2$
6	Fe^{2+}, Co^{3+}	$t_{2g}^4e_g^2$	$^5T_{2g}$	$S = 2$	t_{2g}^6	$^1A_{1g}$	$S = 0$
7	Co^{2+}	$t_{2g}^5e_g^2$	$^4T_{1g}$	$S = 3/2$	$t_{2g}^6e_g^1$	^2E_g	$S = 1/2$

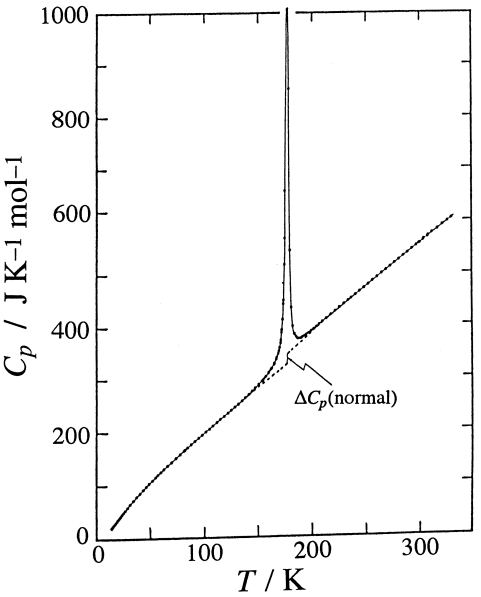

Fig. 4. Molar heat capacity of the iron(II) spin crossover complex $[Fe(NCS)_2(phen)_2]$. Broken curves indicate the normal heat capacities (Ref. 23, 24).

force leading to temperatue-induced spin crossover transition would be a change in the spin multiplicity.

However, in 1974, Sorai and Seki[23,24] measured heat capacities of the spin crossover Fe(II) complexes, $[Fe^{II}(NCS)_2(phen)_2]$ and $[Fe^{II}(NCSe)_2(phen)_2]$, for the first time, and objected to this interpretation. After that, we have developed calorimetric studies for a variety of spin crossover systems, in which spin transition takes place either cooperatively or non-cooperatively, and revealed many important aspects inherent in the spin crossover phenomena. In this article, those thermodynamic studies on spin crossover complexes containing Fe(II), Fe(III), or Cr(II) ions are described in turn.

3.1 First Calorimetric Study on Spin Crossover Phenomena. The first spin crossover complexes calorimetrically studied are Fe(II) complexes, $[Fe(NCS)_2(phen)_2]$ and $[Fe(NCSe)_2(phen)_2]$. As depicted in Fig. 4, we found a phase transition for $[Fe(NCS)_2(phen)_2]$ at 176.29 K with an entropy change of $\Delta S = (48.8 \pm 0.7)$ J K^{-1} mol^{-1}. This entropy value is extremely large in comparison with the entropy gain, $\Delta S = R \ln 5 = 13.38$ J K^{-1} mol^{-1}, expected for a conversion from singlet at the low-spin (LS) state to quintet at the high-spin (HS) state. It should be remarked here that the change in the orbital degeneracies between the LS and HS states does not generally contribute to the entropy gain at the spin crossover transition because the orbital degeneracy, if any, has been lifted by the Jahn–Teller distortion to give a non-degenerate orbital in the resultant lower symmetry. Strictly speaking, therefore, the distorted ligand field is not a genuine octahedral O_h but is a tetragonal D_{4h} or has even lower symmetry. As the spin crossover involves a transfer of two electrons between the e_g and t_{2g} orbitals, the metal-to-ligand bond distances change remarkably, becoming about 0.2 Å shorter in the LS state. This brings about a drastic change in the density of vibrational states, mainly the metal-ligand skeletal vibrational modes.[25] Thus, the transition entropy involves a big contribution from the non-electronic vibrations and the lattice heat capacity exhibits a discontinuity at the transition temperature. As shown in Fig. 4, the present complex $[Fe(NCS)_2(phen)_2]$ brought about a jump of ΔC_p(normal) = 18.7 J K^{-1} mol^{-1}. Based on variable-temperature IR spectroscopy, we could interpret the excess entropy beyond the contribution from the spin multiplicity and the heat capacity jump at the transition temperature in terms of the phonon contribution. Sorai and Seki[24] concluded that the temperature-induced spin crossover is an entropy-driven phenomenon and a coupling between the electronic states and the phonon system plays a fundamental role in the spin crossover transition occurring in the solid state. This concept has long been accepted.

3.2 Chemical Influences on Spin Crossover Phenomena. The spin transition temperature 176.29 K for $[Fe(NCS)_2(phen)_2]$ is drastically shifted to 231.26 K for $[Fe(NCSe)_2(phen)_2]$, in which a sulfur atom of the monodentate ligand NCS, locating far from the central iron atom, is replaced by a selenium atom. As mentioned above, since the spin crossover is the entropy-driven phenomenon, the spin transition temperature is principally determined by compensation of the energy difference caused by a change in the ligand-field strength with the entropy term $T\Delta S$ mainly originating in the phonon system. This is the reason for the large shift of spin transition temperature. In such a way, spin crossover behavior occurring in the solid state is sensitively influenced by chemical and physical factors.[26]

The spin crossover Fe(II) complex $[Fe^{II}(2\text{-pic})_3]X_2$ (2-pic = 2-aminomethylpyridine namely 2-picolylamine; X = Cl, Br, I) reported by Renovitch and Baker[27] is an appropriate material to examine various chemical influences. The magnetic behavior of this series of complexes markedly depends upon the anion present, though the anion is not coordinated to the central iron atom. In the course of ^{57}Fe Mössbauer spectroscopic study, my colleagues and I[28] found that the complex prepared from a solution always led to a compound having solvate molecule(s) such as $[Fe(2\text{-pic})_3]Cl_2\cdot$(solv) (solv = H_2O, $2H_2O$, CH_3OH, C_2H_5OH). The solvate molecule was found to be stoichiometrically amalgamated in the crystal lattice.[29–36] As shown in Fig. 5, the temperature dependence of the high-spin fraction f_{HS} determined on the basis of ^{57}Fe Mössbauer

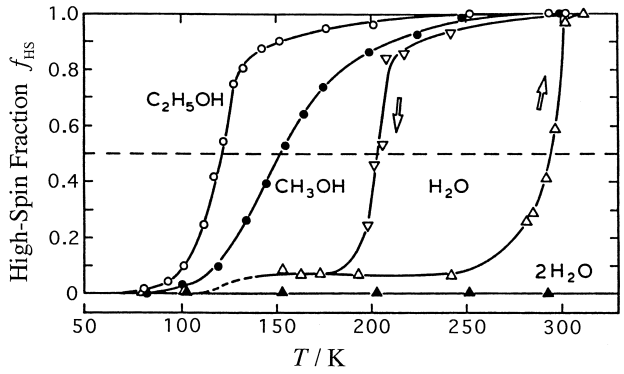

Fig. 5. Temperature dependence of the high-spin area fraction f_{HS} in the spin crossover complexes with different solvate molecules, $[Fe(2\text{-pic})_3]Cl_2 \cdot (solv)$ [solv = H_2O (△,▽), $2H_2O$ (▲), CH_3OH (●), C_2H_5OH (○)] (Ref. 28).

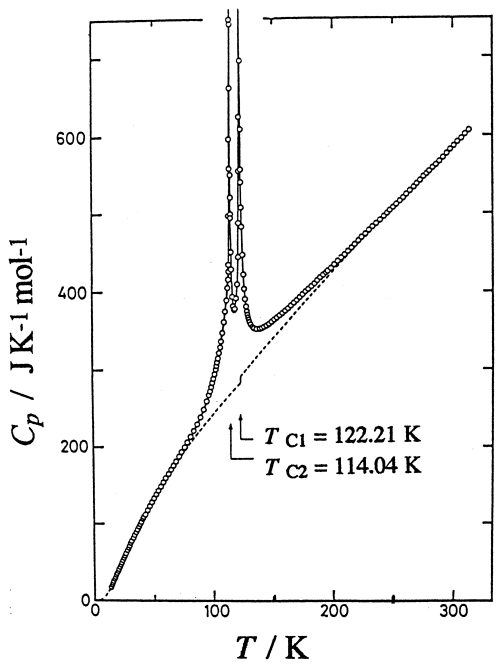

Fig. 6. Molar heat capacity of $[Fe(2\text{-pic})_3]Cl_2 \cdot C_2H_5OH$. Broken curves indicate the normal heat capacities (Ref. 37).

spectroscopy[28] was significantly different for each of these solvate crystals. When the solvate molecule is ethanol, the spin state transformation occurs rather abruptly. For the methanol solvate crystal, the spin crossover proceeds gradually over a wide temperature region. On the other hand, the monohydrate exhibits a large hysteresis concerning spin crossover. If we simply define the spin transition temperature as the temperature at which f_{HS} becomes 0.5, it is 295 K on heating, while it is 204 K on cooling, for the monohydrate. In contrast to this, the dihydrate remains as a low-spin complex and thus does not exhibit a spin transition. A noticeable influence of the non-coordinating solvate molecule $C_nH_{2n+1}OH$ on spin crossover behavior is seen in the drastic change in the transition temperature with the number of carbon atoms n: 121.5 K for $n = 2$, 153 K for $n = 1$, and 295 K for $n = 0$. This is accounted for in terms of a combined action of both the hydrogen-bond formation between the ligand and the intervening solvent molecule and a change in the relevant phonon system caused by different packing geometry and/or some crystallographic change.

In order to elucidate the spin crossover behavior of these complexes from energetic and entropic viewpoints, we measured their heat capacities by adiabatic calorimetry. Figure 6 shows temperature dependence of the molar heat capacity[37] of $[Fe(2\text{-pic})_3]Cl_2 \cdot C_2H_5OH$. This complex exhibited two heat capacity peaks due to phase transitions at 114.04 K and 122.21 K. As the peak temperatures agree with the spin transition temperature estimated from the Mössbauer spectroscopy, these two peaks are closely related to the spin crossover event. The observation of double peaks accords with the reinvestigation of Mössbauer spectroscopy and magnetic susceptibility measurements by Gütlich and his collaborators,[38] showing that a two-step spin conversion in the crossover region occurs at 114.0 K and 120.7 K. Sasaki and Kambara[39] suggested a theoretical model for the two-step spin crossover assuming a sublattice structure for the HS and LS complexes, between which a quasi "antiferromagnetic" interaction is assumed. Real et al.[40] also supported the short-range antiferromagnetic interactions as the source of step-like spin crossover. Recent interpretation by Spiering et al.[41,42] is based on a short-range interaction which is present in addition to the long-range elastic interaction between the spin-changing molecules. A two-step spin crossover phenomenon has been found in other complexes; one recent example is seen in tris(4,4′-bis-1,2,4-triazole)iron(II) diperchlorate.[43]

The broken curves drawn in Fig. 6 gives the normal heat capacities determined by a effective frequency distribution method.[44] Integration of the excess heat capacity beyond the normal heat capacity curves with respect to T and ln T gives the enthalpy gain ΔH and the entropy gain ΔS due to the phase transition, respectively. Table 3 summarizes ΔH, ΔS, and the heat capacity jump ΔC_p(normal) at the transition temperature for the spin crossover complexes studied calorimetrically. The observed ΔS was 50.6 J K^{-1} mol^{-1}, which is much larger than the entropy gain R ln 5 (= 13.4 J K^{-1} mol^{-1}) due to the change in the spin manifold from singlet (LS state) to quintet (HS state). The X-ray structural study[30,33] revealed that the ethanol solvate molecule is jumping in the crystal lattice among three positions with the probabilities 3:2:2 in the HS phase. This dynamic reorientation contributes to the entropy the amount 9.0 J K^{-1} mol^{-1} [= $-R(3/7)$ ln (3/7) − 2R (2/7) ln (2/7)]. The remaining entropy 28.2 (=50.6 − 13.4 − 9.0) J K^{-1} mol^{-1} was accounted for in terms of the phonon entropy mainly due to the six fundamental skeletal vibrational modes of the $[FeN_6]$ core.[37]

When the ethanol solvate molecule is substituted by methanol, the resultant crystal $[Fe(2\text{-pic})_3]Cl_2 \cdot CH_3OH$ exhibits a quite different spin crossover behavior. As illustrated in Fig. 7, this complex gives rise to a broad heat capacity peak centered around 150 K.[45] The entropy gain due to the anomaly is 59.5 J K^{-1} mol^{-1}, which is of the same order of magnitude as the ethanol solvate complex (50.6 J K^{-1} mol^{-1}). As widely accepted nowadays, temperature-induced spin-crossover phenomena are classified into two types: one is the so-called "abrupt type" in which the spin state conversion between LS and HS states takes place within a narrow temperature range less than about

Table 3. Thermodynamic Quantities Associated with Spin Crossover Phenomena

Ion	Compound	T_{trs}	ΔH	ΔS	ΔC_p(normal)	Spin entropy
		K	kJ mol^{-1}	J K^{-1} mol^{-1}	J K^{-1} mol^{-1}	J K^{-1} mol^{-1}
Fe^{2+}	$[Fe(NCS)_2(phen)_2]$	176.29	8.60 ± 0.14	48.8 ± 0.7	18.7	R ln (5/1) = 13.38
S(LS) = 0	$[Fe(NCSe)_2(phen)_2]$	231.26	11.60 ± 0.44	51.2 ± 2.3	45.0	
S(HS) = 2						
	$[Fe(2\text{-pic})_3]Cl_2\cdot$(solv)					
	solv = C_2H_5OH	114.04, 122.21	6.14	50.6	7.8	
	solv = CH_3OH	around 150	8.88	59.5		
	solv = H_2O	280	17.1	59.4		
Fe^{3+}	$[Fe(acpa)_2]PF_6$	around 190	7.03	36.2		R ln (6/2) = 9.13
S(LS) = 1/2	$[Fe(3MeO\text{-}salenEt)_2]PF_6$					
S(HS) = 5/2	As-prepared sample	161.12, 162.02	5.89	36.6	29.9	
	Perturbed sample	161.17	4.94	31.1	21.4	
	Recrystallized sample	162.31	5.94	36.7	28.2	
	$[Fe(3EtO\text{-}salenAPA)_2]ClO_4\cdot$(solv)					
	solv = C_6H_6	187	7.08 ± 0.35	34.8 ± 1.5		
	solv = C_6H_5Cl	188	6.34	36.1		
	solv = C_6H_5Br	around 165	7.99	40.4		
	solv = o-$C_6H_4Cl_2$	around 150	5.38	39.5		
Cr^{2+}						
S(LS) = 1	$[CrI_2(depe)_2]$	171.45	6.69 ± 0.03	39.5 ± 0.2	(ca. 10)	R ln (5/3) = 4.25
S(HS) = 2						

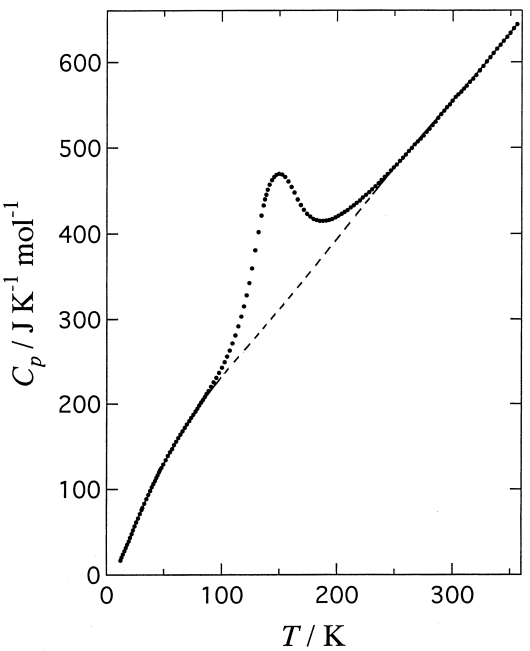

Fig. 7. Molar heat capacity of $[Fe(2\text{-pic})_3]Cl_2\cdot CH_3OH$. Broken curve indicates the normal heat capacity (Ref. 45).

10 K and the other is the "gradual type" in which the spin crossover proceeds over a wider temperature range than 100 K. The spin crossover complex $[Fe(2\text{-pic})_3]Cl_2\cdot CH_3OH$ corresponds to the gradual type. As demonstrated in this paper (see Table 3), the transition entropy largely exceeds the spin entropy due to a change in the spin manifold regardless of the type of spin crossover. The factor governing the abruptness is the degree of cooperativity concerning the spin state conversion. This subject will be discussed in section 3.6.

Based on ^{57}Fe Mössbauer spectroscopy, my colleagues and I[28] reported that the mono-hydrate complex $[Fe(2\text{-pic})_3]Cl_2\cdot H_2O$ exhibits a spin crossover at 204 K on cooling and at 295 K on heating, manifesting a large thermal hysteresis of about 90 K. In order to confirm this fact, we recorded its thermogram by DTA (differential thermal analysis) and measured its heat capacity by adiabatic calorimetry.[46] As the result, it turned out that the thermal hysteresis is not genuine but only apparent. Cooling DTA-run for the as-grown sample always gave rise to an exothermic peak at 199 K and the succeeding heating run showed an endothermic peak at 211 K, while no anomaly was observed around 295 K. This thermal behavior is quite different from the previous result derived from Mössbauer spectroscopy.[28] Since the elemental analysis for C, H, and N elements agreed well with the calculated values, it was not likely that the different spin crossover behavior originates in chemical purity. We then decided to measure precisely its heat capacity by use of an adiabatic calorimeter.

The sample was first cooled from room temperature to 10 K. In the course of cooling, an exothermic peak due to a transition to a low-temperature LS-phase was detected at 200 K. Heat capacity measurement was started for the specimen thus cooled. Although a heat capacity peak originating in the phase transition from the LS- to HS-states was actually observed around 220 K, the magnitude of this peak depended on the heat treatment done for the specimen. When the sample was annealed around 200 K, it was stabilized to the stable LS-phase with evolution of heat and, as a result, the phase transition at

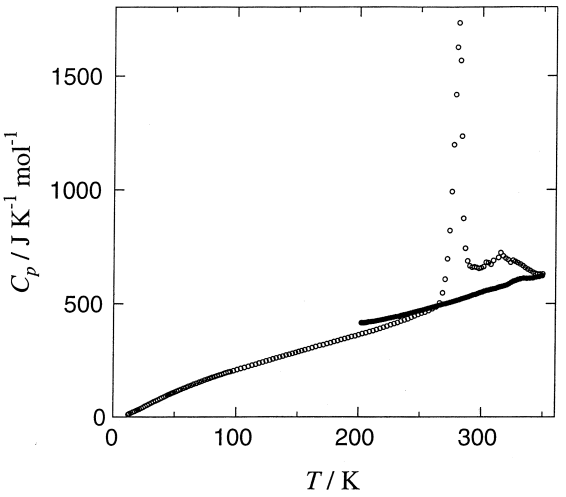

Fig. 8. Molar heat capacity of $[Fe(2\text{-pic})_3]Cl_2 \cdot H_2O$. Open circles imply the data determined in the stable phases, while solid circles correspond to the undercooled HS-phase (Ref. 46).

220 K disappeared. Instead, as shown in Fig. 8, a large heat capacity peak arising from the transition from the stable LS- to HS-phase was observed at 280 K. This phase transition was accompanied by a broad hump centered at 320 K. The enthalpy and entropy gains due to the spin crossover transition at 280 K and the hump at 320 K are $\Delta H = 17.1$ kJ mol^{-1} and $\Delta S = 59.4$ J K^{-1} mol^{-1}. Relationships between these phases are schematically shown in Fig. 9. The phase transition at 280 K was always undercooled to about 200 K (path: A–B–C–D) and the undercooled HS-state was transformed to a metastable LS-phase around 200 K (path: D–E). When the heating rate is high, this phase was transformed to the undercooled HS-phase at 210 K (path: E–F–C–B–A). However, when the specimen was treated slowly around this temperature region, it was stabilized to the stable LS-phase around 200 K (path: F–G). Since the time required for data acquisition is extremely long for both Mössbauer spectroscopy and adiabatic calorimetry, the sample was always stabilized to the stable LS-phase around 200 K. The data shown by open circles in Fig. 8 correspond to the heat capacities for the stable phases determined along the path I–G–B–A, while the data shown by solid circles imply the heat capacities for the undercooled HS-phase along the path D–C–B–A. This new finding of the existence of the metastable LS-phase by the calorimetric study[46] clarified the cause of the apparent thermal hysteresis spanning between 204 K and 295 K found at the Mössbauer experiment,[28] corresponding to the paths A–B–C–D–E–F–G–I and I–G–B–A.

3.3 Influence of Metal Dilution. As described above, on the basis of precise heat capacity measurements, Seki and I[23,24] have suggested that the spin transitions in $[Fe(NCS)_2(phen)_2]$ and $[Fe((NCSe)_2phen)_2]$ are cooperative phenomena proceeding via significant coupling between the electronic state and the phonon system and that the spin conversion occurs simultaneously in a group of molecules forming a "cooperative domain". For more complete understanding of this picture of cooperative spin transition, studies on solid solutions in which spin crossover complexes are diluted with non-crossover complexes will surely provide useful clues. Renovitch and Baker[27]

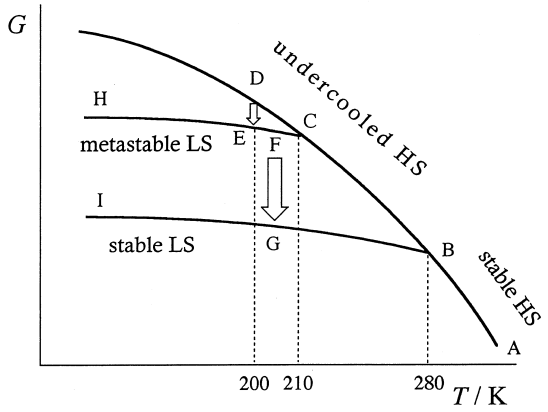

Fig. 9. Gibbs energy relationship between various LS- and HS-phases realized in the spin crossover complex $[Fe(2\text{-pic})_3]Cl_2 \cdot H_2O$.

briefly reported that even the chloride salt of the iron complex diluted with 85 mol% of the zinc complex, $[Fe_{0.15}Zn_{0.85}(2\text{-pic})_3]Cl_2$, exhibits similar magnetic behavior to that of the pure iron complex. Stimulated by this finding, my colleagues and I[47] developed a Mössbauer effect study for the solid solutions $[Fe_xZn_{1-x}(2\text{-pic})_3]Cl_2 \cdot C_2H_5OH$ ($x = 0.2$, 0.6, 0.8, 1.0). The phase transition temperature T_C defined by the area fraction of the Mössbauer spectra was 121.5 K, 114.5 K, 106.5 K, and 90.0 K for the systems with $x = 1.0$, 0.8, 0.6, and 0.2, respectively. A linear relation between T_C and x was obtained as

$$T_C(x)/K = 40x + 82.$$

Gütlich et al.[48] extended the Mössbauer study to more diluted solid solutions having $x = 0.15$, 0.029, and 0.0009. As reproduced in Fig. 10, the concentration dependence of the spin

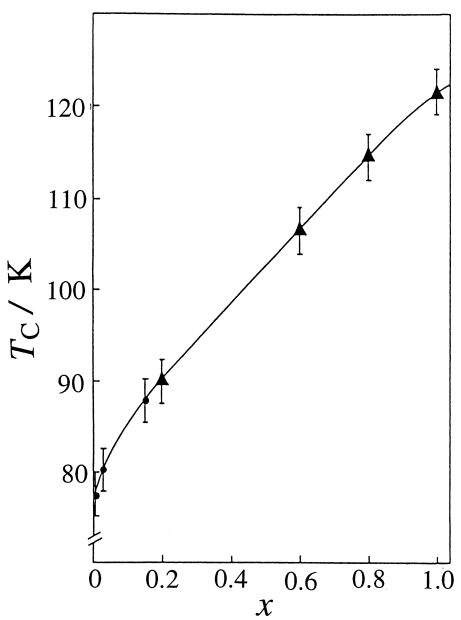

Fig. 10. Concentration dependence of the spin transition temperature (T_C) for $[Fe_xZn_{1-x}(2\text{-pic})_3]Cl_2 \cdot C_2H_5OH$. ▲: Sorai et al. (Ref. 47), ●: Gütlich et al. (Ref. 48).

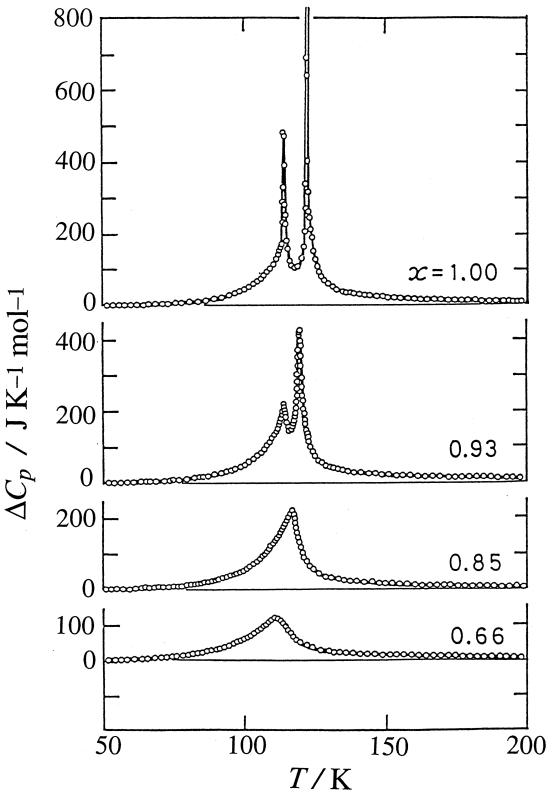

Fig. 11. Concentration dependence of the excess heat capacities arising from the spin crossover transition for $[Fe_xZn_{1-x}(2\text{-pic})_3]Cl_2{\cdot}C_2H_5OH$ (x = 0.66, 0.85, 0.93, 1.00) (Ref. 49).

Table 4. The Entropy Gain ΔS due to the Spin Crossover Transition in $[Fe_xZn_{1-x}(2\text{-pic})_3]Cl_2{\cdot}C_2H_5OH$ (Ref. 49)

x	ΔS (x, obsd)	ΔS (x, calcd)
	J K^{-1} mol^{-1}	J K^{-1} mol^{-1}
1.00	50.6	50.8
0.93	48.2	47.2
0.85	42.4	43.1
0.66	33.3	33.5
0.00	0	0

crossover temperature is almost linear and seems to show that the pure zinc complex (x = 0.0) had a spin transition around 80 K. This is quite peculiar because the zinc complex is not a spin-crossover complex at all. As discussed later, this unusual concentration dependence originates in the phonon-assisted mechanism inherent in the spin crossover transition.

Figure 11 illustrates the excess heat capacity ΔC_p for the spin crossover transition in $[Fe_xZn_{1-x}(2\text{-pic})_3]Cl_2{\cdot}C_2H_5OH$ (x = 0.66, 0.85, 0.93, 1.00).[49] The temperature interval of the two-step transition and the peak intensities are diminished as x is decreased. The averaged transition temperature follows well the equation given above. As listed in Table 4, the observed entropy gains ΔS (x, obsd.) are well reproduced by the following contribution:

$$\Delta S\ (x, \text{calcd.}) = x\,(R \ln 5 + R \ln 3 + 28.24\ \text{J K}^{-1}\ \text{mol}^{-1}).$$

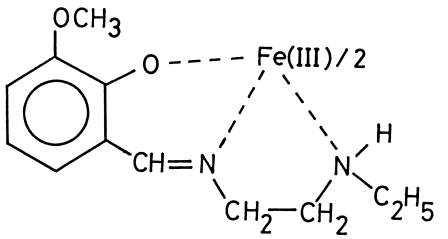

Fig. 12. Coordination geometry of the iron(III) spin crossover complex $[Fe(3MeO\text{-}salenEt)_2]PF_6$.

The first term on the right hand side of the equation corresponds to the entropy due to the change in the spin manifold, the second term stands for the configurational entropy of the ethanol solvate molecule, and the third term gives the phonon entropy due to the change in metal–ligand bond lengths. It is of great interest that both the transition temperature T_C and the entropy gain ΔS (x, obsd.) show linear concentration dependence over the whole range of x. This fact strongly suggests that the spin crossover takes place by a long-range interaction communicated through normal modes of lattice vibration.[47]

Similar studies on the metal dilution were made by Jakobi et al.[50,51] for partially deuterated complexes $[Fe_xZn_{1-x}(2\text{-pic-}ND_2)_3]Cl_2{\cdot}C_2H_5OD$ (x = 1.0, 0.91, 0.78, 0.68, 0.60, 0.46) on the basis of DSC measurements and for $[Fe_{0.73}Zn_{0.27}(2\text{-pic})_3]Cl_2{\cdot}C_2H_5OH$ based on a relaxation microcalorimeter.[52]

3.4 Influence of Grinding and Pressure. Spin crossover behavior is influenced by mechanical treatment. Hendrickson and his collaborators[53–55] reported unusual effects appearing in a microcrystalline sample of iron(III) complex $[Fe^{III}(3MeO\text{-}salenEt)_2]PF_6$, the coordination geometry of which is shown in Fig. 12. As this complex is cooled from room temperature, black HS-state is transformed around 160 K to blue LS-state. Grinding a microcrystalline sample of this compound leads to an incompleteness of the transition; some complexes persist in the HS-state even at low temperatures. The transition also becomes more gradual upon sample grinding, and more LS-molecules form in the ground samples at higher temperatures compared to the unground samples. These effects are mainly caused by increased lattice defects and imperfection of crystal lattices.

Although it is difficult to quantitatively assess the degree of defect or imperfection, comparative studies of various physical quantities between as-prepared and ground samples surely provide useful clue to understand the mechanism of spin crossover. We measured heat capacities of the following three kinds of samples:[56] (1) as-prepared sample, (2) the sample carefully ground for 3 min with mortar and pestle (designated hereafter as perturbed sample), and (3) the sample obtained by dissolving the perturbed sample in methanol and then by evaporating a methanol solution to dryness (designated as recrystallized sample). These three samples likewise gave rise to a phase transition due to the spin crossover around 160 K. The as-prepared sample exhibited a heat capacity anomaly consisting of double peaks at 161.12 K and 162.07 K. Contrary to this, the perturbed sample exhibited a single peak at 161.17 K and the recrystallized sample gave a sharp peak at 162.31 K. Since the as-prepared sample was a fine powder and the crystal quality seems to be not so high compared to that of the recrystallized

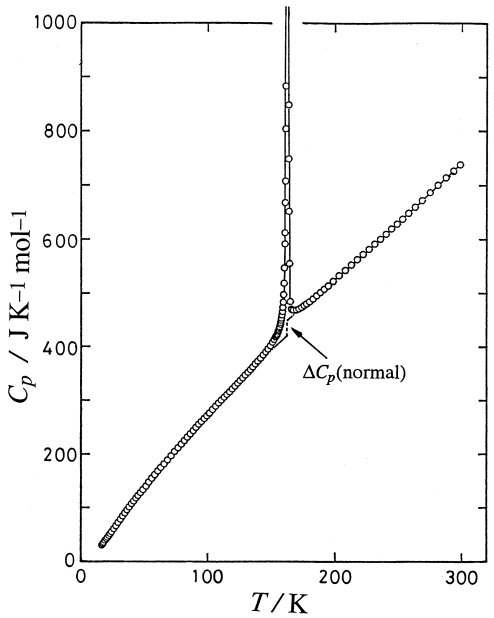

Fig. 13. Molar heat capacity of the iron(III) spin crossover complex [Fe(3MeO-salenEt)$_2$]PF$_6$. The broken curves drawn in the vicinity of the phase transition region imply the normal heat capacities (Ref. 56).

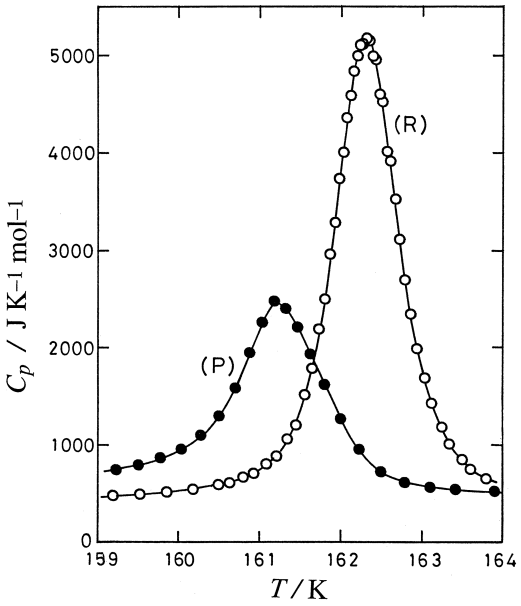

Fig. 14. Molar heat capacities of [Fe(3MeO-salenEt)$_2$]PF$_6$ in the vicinity of the spin crossover transition for the perturbed (P) and recrystallized (R) samples (Ref. 56).

sample, we shall discard this sample from the following discussion. Figure 13 shows the molar heat capacity of the recrystallized sample. As in the case of usual spin crossover complexes, the normal heat capacity brought about a discontinuity of ΔC_p(normal) = 28.2 J K^{-1} mol^{-1}. The transition entropy (36.7 J K^{-1} mol^{-1}) is well accounted for in terms of the sum of the spin entropy R ln (6/2) (= 9.13 J K^{-1} mol^{-1}) and the phonon entropy (25.5 J K^{-1} mol^{-1}), which is estimated on the basis of variable-temperature IR spectroscopy and the theoretical assignments of the metal-ligand skeletal vibrations for related complexes.

As seen in Fig. 14, the peak height is remarkably reduced only by a 3 min grinding. The enthalpy and entropy gains at the phase transition for the perturbed sample are by 15 per cent smaller than those of the recrystallized sample (see Table 3). From this investigation, one can understand that the spin crossover is remarkably influenced by the grain size, crystal defect, lattice imperfection, and so on. This fact supports the idea[24] so far proposed that the mechanism of spin crossover involves a strong coupling between the electronic state and the phonon (or elastic) system.

Although grinding crystals inevitably involves a change in the crystal quality, varying hydrostatic pressure does not principally lead to the damage of a crystal. In that sense, experiments under applied pressure are more quantitative to assess. Since the complex molecules are bigger in the HS-state than in the LS-state, one can expect that increasing the pressure would favor the LS-state.[57] Although the pressure effect is of great interest, no calorimetric investigations have been reported.

3.5 Spin Crossover in Non-Iron Complex. The complexes which give rise to the spin crossover phenomena in an octahedral symmetry are not restricted to iron(II) and iron(III) complexes (see Table 2). One of non-iron spin crossover com-

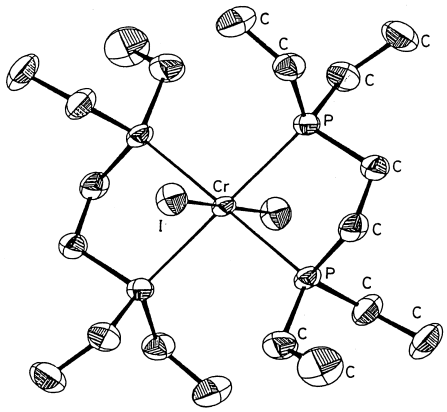

Fig. 15. Molecular structure of [CrI$_2$(depe)$_2$] at room temperature (Ref. 58).

plexes is bis[1,2-bis(diethylphosphino)ethane]diiodochromium(II) ([CrI$_2$(depe)$_2$] for short).[58] The molecular structure of this complex at room temperature is shown in Fig. 15.[58] The central chromium ion is nearly octahedrally coordinated by four phosphorus atoms belonging to two phosphine ligands and by two iodide ions. The magnetic moment of this complex is characteristic of the LS-state with the spin quantum number $S = 1$ at low temperatures, while it becomes the value characteristic of the HS-state with $S = 2$ at high temperatures. Transformation between these two spin states occurs abruptly around 170 K. Figure 16 illustrates the molar heat capacity of this complex.[59] A sharp peak due to the spin crossover was observed at 171.45 K. Since this temperature corresponds to the temperature at which the magnetic moment is altered from the LS- to HS-values, the present heat capacity anomaly obviously arises from the spin-state transformation.

The entropy acquisition due to the phase transition is shown

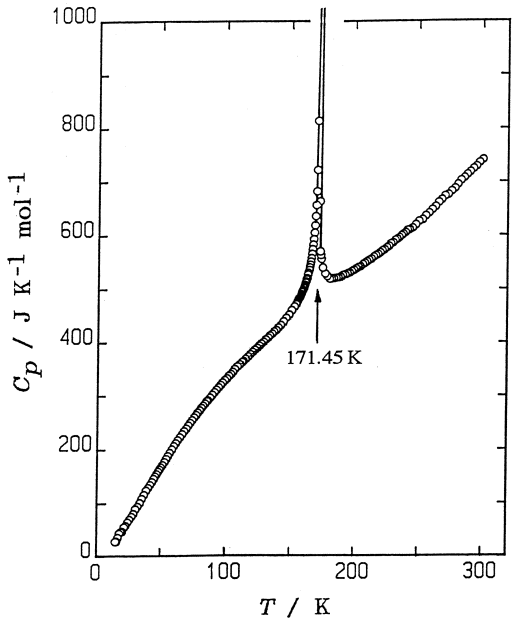

Fig. 16. Molar heat capacity of the chromium(II) spin crossover complex $[CrI_2(depe)_2]$ (Ref. 59).

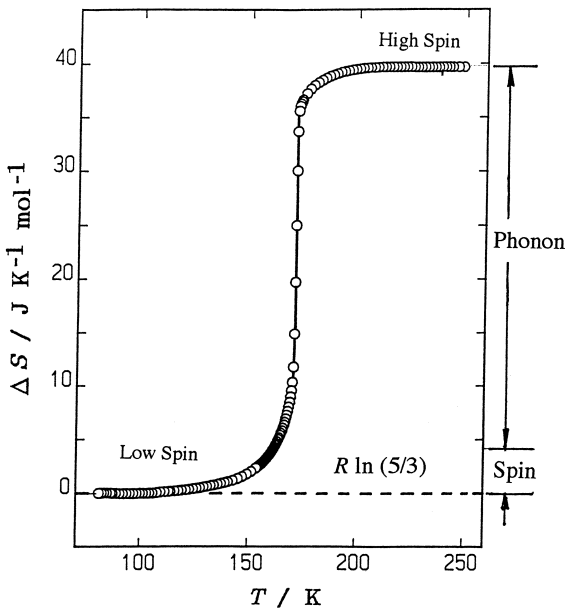

Fig. 17. Entropy acquisition with the spin crossover transition of $[CrI_2(depe)_2]$.

in Fig. 17. The ground term of Cr(II) ion in O_h symmetry is $^3T_1$ and ^5E in the LS- and HS-states, respectively. As described in section 3.1, the orbital degeneracies between the LS- and HS-states do not generally contribute to the entropy gain at the spin crossover transition because the orbital degeneracy has been lifted by the Jahn–Teller distortion to give a non-degenerate ground orbital in the resultant lower symmetry. The total transition entropy was (39.5 ± 0.2) J K^{-1} mol^{-1}. The observed entropy is much greater than the entropy gain at the change in the spin manifold, R ln (5/3) = 4.25 J K^{-1} mol^{-1}. However, this fact is not surprising because the spin-crossover

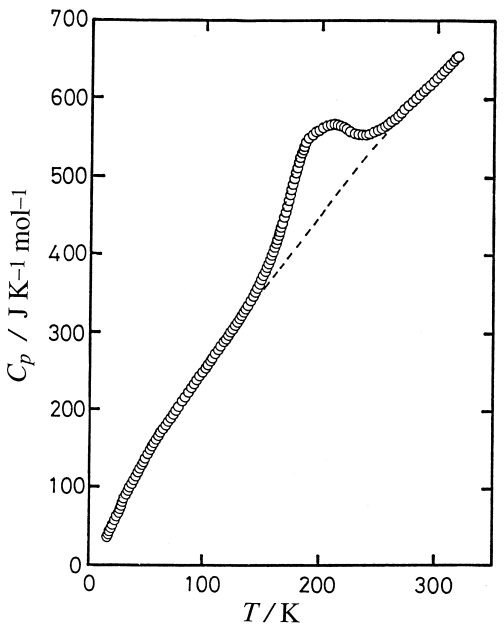

Fig. 18. Molar heat capacity of the iron(III) spin crossover complex $[Fe(acpa)_2]PF_6$. The broken curve stands for the normal heat capacity (Ref. 60).

transition always involves a dominant contribution from a change in the phonon entropies between two spin states. Vibrational spectra of this complex exhibited drastic changes in the skeletal modes. The main part of the transition entropy, about 35 J K^{-1} mol^{-1}, can be accounted for in terms of the change in the phonon system.

3.6 Gradual Spin Crossover Phenomena. As widely recognized, spin-crossover transformations can phenomenologically assume two limiting cases: one is the so-called abrupt type in which the spin-state transformation takes place abruptly within a narrow temperature range of a few kelvins and the other is the gradual type in which the spin-crossover occurs gradually over a wide temperature range, typically greater than 100 K.

The first calorimetric measurement of the gradual type was made for the iron(III) spin crossover complex $[Fe(acpa)_2]PF_6$ [Hacpa = *N*-(1-acetyl-isopropylidene)(2-pyridylmethyl)-amine].[60] This complex shows fast electronic relaxation between $^2T_{2g}$ (S = 1/2) and $^6A_{1g}$ (S = 5/2) in comparison with the ^{57}Fe Mössbauer lifetime (10^{-7} s). As reproduced in Fig. 18, an unusually broad heat capacity peak covering from 120 K to 280 K was observed. The enthalpy and entropy arising from the spin crossover phenomenon were 7.03 kJ mol^{-1} and 36.2 J K^{-1} mol^{-1}, respectively. The entropy gain was well accounted for in terms of the sum (37.7 J K^{-1} mol^{-1}) of the contributions from the change in the spin manifold R ln (6/2) (= 9.1 J K^{-1} mol^{-1}) and from a change in the skeletal normal modes of vibration detected by IR and Raman spectra (28.6 J K^{-1} mol^{-1}). To elucidate the reason for the gradual spin state conversion, Sorai and Seki[24] proposed in 1974 a simple domain model based on the Frenkel theory[61] of heterophase fluctuation in liquids. As schematically shown in Fig. 19, this model assumes that a crystal lattice consists of non-interacting domains with uniform size containing n complexes and that the spin state

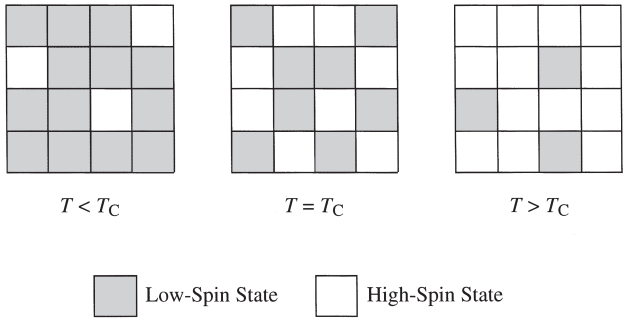

Fig. 19. Schematic drawing of the domain model. The crystal lattice is divided by uniform size of domains containing equal number of spin-crossover complexes. T_C is the transition temperature at which the number of LS-domain becomes equal to that of HS-domain.

conversion in each domain takes place simultaneously. This assumption of independent domains is obviously a consequence of the nucleation-and-growth mechanism inherent in the first-order phase transition. As the number n is decreased, the heat capacity peak due to the spin crossover becomes broader and the cooperativity of the transition becomes weaker. When n takes the extreme value of unity, the system just corresponds to a chemical equilibrium described by the van't Hoff scheme. The existence of such domains was evidenced for $[Fe(2\text{-pic})_3]Cl_2 \cdot C_2H_5OH$ based on EPR measurements in 1990 by Doan and McGarvey.[62] The number of complexes n in a domain estimated for $[Fe(acpa)_2]PF_6$ on the basis of this model was only five, which makes a sharp contrast to 95 and 77 found for the abrupt type complexes $[Fe(NCS)_2(phen)_2]$ and $[Fe(NCSe)_2(phen)_2]$,[24] respectively, and 2000 for $[CrI_2(depe)_2]$.[59] In the case of $[Fe(2\text{-pic})_3]Cl_2 \cdot CH_3OH$, the excess heat capacity ΔC_p is well reproduced by the domain model, when the number of complexes in a domain is 1.5 (Fig. 20).[45] This small number of complexes per domain implies that the cooperativity in this complex is extremely weak or absent.

A homologous series of iron(III) complexes $[Fe(3EtO\text{-}salAPA)_2]ClO_4 \cdot (solv)$ (solv = C_6H_6, C_6H_5Cl, C_6H_5Br, or o-C_6H_4-Cl_2) provide us with interesting example of the gradual type spin crossover, where 3EtO-salAPA$^-$ is the Schiff base condensed from 1 mol of 3-ethoxysalicylaldehyde with 1 mol

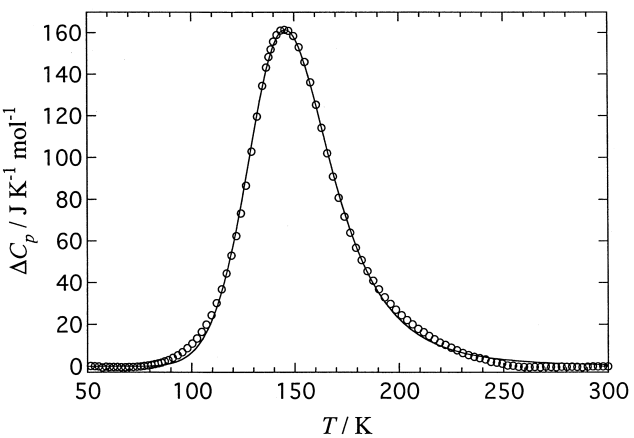

Fig. 20. Excess heat capacity arising from the spin crossover in $[Fe(2\text{-pic})_3]Cl_2 \cdot CH_3OH$ (Ref. 45).

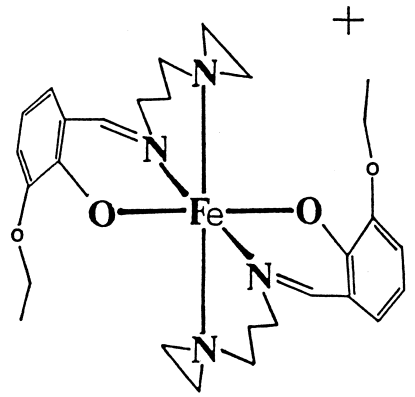

Fig. 21. Molecular structure of the $[Fe(3EtO\text{-}salAPA)_2]^+$ ion.

of *N*-aminopropylaziridine (see Fig. 21). Effective magnetic moments[63] of these complexes exhibit very gradual spin-state transformation over a wide temperature region. In accordance with this feature, they exhibit very broad heat capacity anomalies.[64–67] Figure 22 shows molar heat capacity of the bromobenzene solvate complex. As is expected from the temperature dependence of the magnetic moment,[63,64] this complex brought about a very broad heat capacity anomaly centered around 165 K. A peak at 288.3 K originates in the structural change detected by X-ray diffraction analysis.[64] Excess heat capacity of $[Fe(3EtO\text{-}salAPA)_2]ClO_4 \cdot C_6H_5Br$ beyond the normal heat capacity is shown in Fig. 23. Thermodynamic quantities associated with the broad anomaly and the phase transition at 288.3 K amounted to $\Delta H = 7.99$ kJ mol^{-1} and $\Delta S = 40.4$ J K^{-1} mol^{-1}. Of the observed entropy gain, contribution from the change in the spin manifold is only R ln (6/2) = 9.13 J K^{-1} mol^{-1}. As in the case of other spin crossover complexes, the main part of the remaining entropy can be accounted for in terms of the phonon entropy and a small contribution from the structural change.

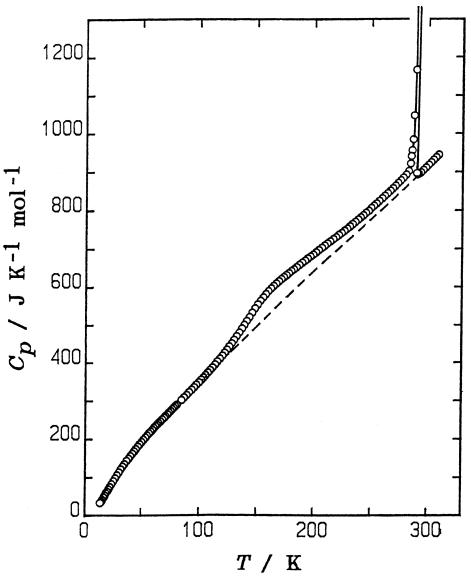

Fig. 22. Molar heat capacity of the spin crossover complex $[Fe(3EtO\text{-}salAPA)_2]ClO_4 \cdot C_6H_5Br$. The broken curve indicates the normal heat capacity (Ref. 67).

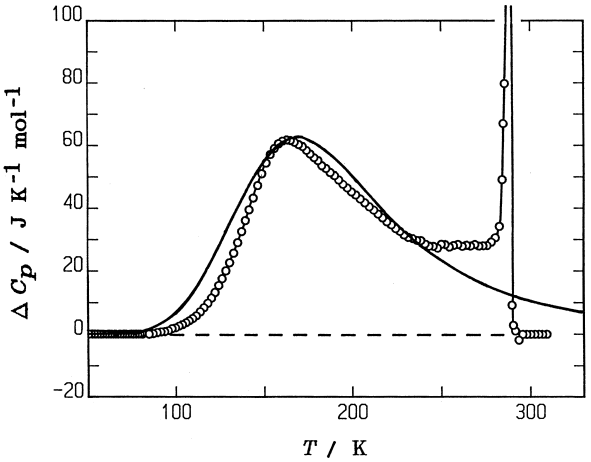

Fig. 23. Excess heat capacity of the spin crossover complex $[Fe(3EtO\text{-}salAPA)_2]ClO_4{\cdot}C_6H_5Br$. The solid curve stands for the theoretical curve based on the van't Hoff equation with $\Delta H = 8.21$ kJ mol^{-1} and $\Delta S = 42.7$ J K^{-1} mol^{-1}, while the observed values are $\Delta H = 7.99$ kJ mol^{-1} and $\Delta S = 40.4$ J K^{-1} mol^{-1} (Ref. 67). The solid line connecting the observed points shown by open circles is only eye-guide.

Let's consider here the cooperativity inherent in the spin-state interconversion. In a dilute solution of spin-crossover complexes, the equilibrium between HS- and LS-states is governed by the Boltzmann distribution function. In the solid state, however, the existence of intermolecular interactions leads to more or less cooperative nature of the spin crossover. We consider now a system in which LS- and HS-species are in thermal equilibrium. When the HS-fraction is f, the LS-fraction becomes $(1 - f)$. The equilibrium constant K is defined by the following equation:

$$K = [f]/[1 - f].$$

The high-spin fraction f can be derived from the experimental magnetic moment μ_{eff} based on the equation:

$$\mu_{\text{eff}}(\text{exptl})^2 = f{\cdot}\mu_{\text{eff}}(\text{HS})^2 + (1 - f){\cdot}\mu_{\text{eff}}(\text{LS})^2.$$

By substituting the HS-fraction f in K with the values determined by this equation, one can determine the value of K as a function of temperature. A plot of ln K against $1/T$ for the present complex provided a straight line. This fact indicates that the spin crossover can be described by a simple equilibrium scheme, just corresponding to the van't Hoff equation:

$$\ln K = -\Delta G/RT = -\Delta H/RT + \Delta S/R,$$

where ΔG is the Gibbs energy difference between the HS- and LS-states, ΔH the enthalpy difference, and ΔS the entropy difference. The least-squares fitting brought about $\Delta H = 8.21$ kJ mol^{-1} and $\Delta S = 42.7$ J K^{-1} mol^{-1}. These values are very close to the observed values calorimetrically determined: $\Delta H = 7.99$ kJ mol^{-1} and $\Delta S = 40.4$ J K^{-1} mol^{-1}.

The excess heat capacity arising from such an equilibrium system can be derived from the following equation:

$$\Delta C_p = \mathrm{d}(f{\cdot}\Delta H)/\mathrm{d}T = (\Delta H)^2\exp(-\Delta H/RT + \Delta S/R)/\{RT^2[1 + \exp(-\Delta H/RT + \Delta S/R)]^2\}.$$

The observed heat capacity anomaly of $[Fe(3EtO\text{-}salAPA)_2]ClO_4{\cdot}C_6H_5Br$ is compared with the calculated value in Fig. 23. The former is given by open circles while the latter is given by the solid curve. The broad anomaly centered around 165 K can be satisfactorily reproduced by the van't Hoff equation. In other words, the gradual type spin-state transformation in the present complex takes place not cooperatively but in a simple equilibrium scheme. This fact that the spin crossover can likewise proceed even non-cooperatively rationalizes the experimental result described in section 3.3 that the iron spin-crossover complex extremely diluted with zinc analogue $[Fe_xZn_{1-x}(2\text{-}pic)_3]Cl_2{\cdot}C_2H_5OH$ ($x = 0.0009$) still exhibits a spin-state conversion in Mössbauer spectroscopy.[48]

Finally, it should be remarked that the rate of spin state interconversion also governs the level of abruptness of the spin state transformation. It is generally true that when the rate of spin-state interconversion sensed by Mössbauer spectroscopy is great, the complex exhibits gradual type spin-crossover, while for the complexes characterized by slow rate of spin-state conversion one can expect an abrupt phase transition.

4. Intramolecular Electron Transfer in the Mixed-Valence Complexes

4.1 Theoretical Background. Complexes which involve several identical elements characterized by different oxidation states are called mixed-valence compounds.[68–72] One of the well-known examples is the set of oxo-centered trinuclear metal acetate complexes with the formula $[M^{III}_2M^{II}O(O_2CCH_3)_6L_3]{\cdot}(\text{solv})$ (L: monodentate ligand, solv: solvate molecule). Figure 24 shows the iron complex $[Fe_3O(O_2CCH_3)_6(py)_3]$ (py: pyridine) at the valence-detrapped state.[73] Each of three transition-metal ions is octahedrally coordinated by the central oxygen ion, a neutral pyridine, and four acetate ligands. Many of these complexes have been

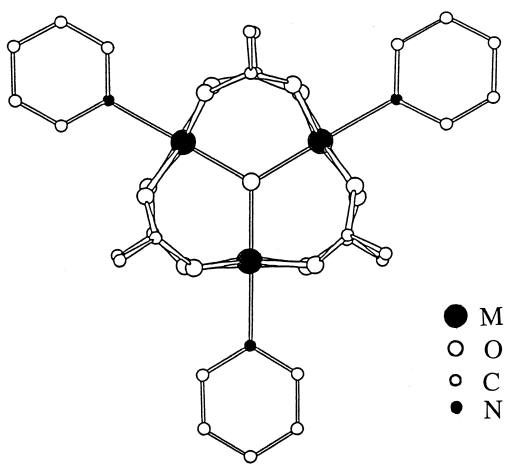

Fig. 24. Molecular structure of the oxo-centered trinuclear basic metal acetate having a formula $[M^{III}_2M^{II}O(O_2CCH_3)_6(py)_3]$ with D_{3h} symmetry in the valence-detrapped state (Ref. 73).

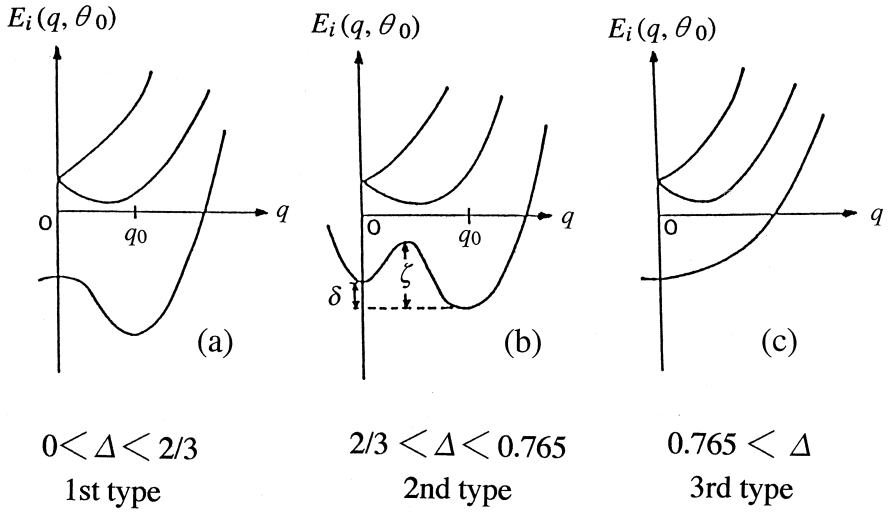

Fig. 25. Three types of the energy profiles $E_i(q,\theta_0)$ for different values of Δ along the direction of a M–O bond ($\theta_0 = 0$, $2\pi/3$, or $-2\pi/3$), where q is the amplitude of distortion (Ref. 81).

shown to convert from being valence-trapped at low temperatures to valence-detrapped at high temperatures.[74–77] One of the remarkable discoveries at the initial stage of the investigations was that the solvate molecules that are not explicitly coordinated to the central metal ions have a dramatic effect on the electron-transfer rate, while the non-solvated analogue $[Fe_3O(O_2CCH_3)_6(py)_3]$ remains in a valence-trapped state even at 315 K.[74,75]

Formally speaking, the oxidation state of two metal ions in a trinuclear mixed-valence M_3O complex is M(III), while that of the remaining ion is M(II). The M(II) ion is characterized by having an "extra" d-electron in comparison to the M(III). The electronic state of a free-molecule would be triply degenerated in the sense that the extra d-electron can reside on any one of three metal centers. Intramolecular electron-transfer between the metal centers in a trinuclear mixed-valence complex $M^{III}_2M^{II}O$ is usually treated by a theory incorporating vibronic interactions.[78–80] The extra d-electron residing on the low-oxidation metal center is coupled with the e_g symmetry M_3O stretching vibration via the vibronic interactions. In effect, the vibronic interaction includes a pseudo Jahn-Teller distortion of the molecule. As the result, the degeneracy may be lifted as shown in Fig. 25.[81] Since the thermal energy concerning the present calorimetry is very small, about $300R$ at most, we shall discuss here only the ground electronic state. The appearance of the adiabatic potential energy surfaces for the vibronic states of this complex depends on the value of the electron-transfer integral between two metal ions ω and the vibronic coupling energy λ^2/κ, where κ is the force constant for the e_g stretching vibration and λ is the vibronic coupling constant of the d-electron to the e_g vibrational mode. When $\Delta\ (= \kappa\omega/\lambda^2)$ is in the range $0 < \Delta < 2/3$, there are three vibronic states, as shown in Fig. 25a. The adiabatic potential energy surface for the ground state of the mixed-valence M_3O complex is pictured in Fig. 26a[82] for the case of $\Delta = 0.05$. These three potential minima correspond to three different isosceles triangles of a complex formed by the pseudo Jahn–Teller distortion. In each of these states, the extra d-electron is located mainly on one of the three metal ions. When Δ is in the range $2/3 < \Delta <$ 0.765, a fourth minimum appears on the potential energy surfaces, as shown in Fig. 25b and pictured in Fig. 26b for the case of $\Delta = 0.74$. This fourth configuration newly appearing at $q = 0$ (q: amplitude of distortion) corresponds to a M_3O complex that has an equilateral triangular form, and the extra d-electron is coherently delocalized over all three metal ions. Contrary to these two types, the third type ($0.765 < \Delta$) brings

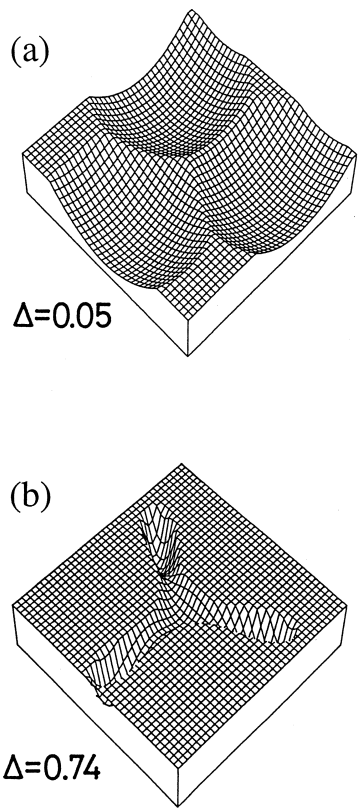

Fig. 26. Three-dimensional drawing of the adiabatic potential energy surface for the ground electronic states of a mixed-valence M_3O complex calculated for two different values of (a) $\Delta = 0.05$ and (b) $\Delta = 0.74$ (Ref. 82).

about only a single minimum at $q = 0$.

The explanation so far made is valid for an isolated single cluster. The situation is altered when mixed-valence complexes are aggregated in a crystal. The rate of intramolecular electron-transfer is seriously affected by environmental effects in the solid state. In particular, solvate molecules that are not explicitly coordinated to the central metal ions but are stoichiometrically amalgamated in the crystal lattice play an important role for the intramolecular electron transfer event.

Entropy gain due to the valence-detrapping phenomenon is straightforwardly related to a change in the number of microscopic states that are thermally accessible for a given mixed-valence complex. At low temperatures, the mixed-valence complex is valence-trapped and has statically one of the isosceles triangular configurations. However, depending on the magnitude of Δ, the dynamically interconverting mixed-valence complexes in the high temperature phase will gain either three or four microscopic states, as shown in Figs. 25 and 26. In the former case, the valence-detrapping gives an entropy gain of R ln 3, whereas in the latter case the entropy gain is R ln 4.

4.2 Phase Transitions in Trinuclear Mixed-Valence Complexes. The mixed-valence trinuclear complexes discussed here are $[M^{III}_2M^{II}O(L2)_6(L1)_3]\cdot(solv)$ (L1: monodentate ligand, L2: bidentate ligand, solv: solvate molecule). We measured heat capacities of $[Fe_3O(O_2CCH_3)_6(py)_3]\cdot(py)$ (**1**),[83,84] $[Mn_3O(O_2CCH_3)_6(py)_3]\cdot(py)$ (**2**),[82,85] $[Fe_3O(O_2CCH_3)_6(py)_3]\cdot(CHCl_3)$ (**3**),[86,87] $[Fe_3O(O_2CCH_3)_6(4\text{-Me-py})_3]\cdot(CHCl_3)$ (**4**),[88] $[Fe_3O(O_2CCH_3)_6(3\text{-Me-py})_3]\cdot(3\text{-Me-py})$ (**5**),[89] and $[Fe_3O(O_2CCH_3)_6(3\text{-Me-py})_3]\cdot(toluene)$ (**6**),[90] together with a solid solution $[Fe^{III}_2Fe^{II}_{0.5}Co^{II}_{0.5}O(O_2CCH_3)_6(py)_3]\cdot(py)$ (**7**)[91] and a non-mixed-valence analogue $[Fe^{III}_2Co^{II}O(O_2CCH_3)_6(py)_3]\cdot(py)$ (**8**).[91] The complexes **1**–**4** commonly crystallize into an identical rhombohedral crystal system with the space group $R32$ in the valence-detrapped high temperature phases. Comparisons of the phase transition behaviors between **1** and **2**, **1** and **3**, and **3** and **4** may provide us with clues to understanding the role of central metal ion, solvate molecule, and monodentate ligand, respectively.

The variable-temperature ^{57}Fe Mössbauer spectra of the complex **1** reported by Hendrickson and his collaborators[74,75] showed dramatic changes with temperature. At temperatures below about 100 K, two quadrupole-split doublets are seen: one characteristic of high-spin iron(II) and the other of high-spin iron(III). As the temperature is increased, an extra doublet appears abruptly around 110 K at the expense of the initial two doublets. This means that the new doublet arises from the electron-delocalized state. The spectrum eventually becomes a single doublet above about 190 K. This fact indicates that the rate of intramolecular electron-transfer exceeds the rate of 10^7 s^{-1} which the Mössbauer technique can sense. Figure 27[83,84] shows the molar heat capacity of this complex. This complex exhibits essentially two kinds of phase transitions: one is a first-order phase transition at about 112 K and the other is a higher-order phase transition around 190 K. Interestingly, the low-temperature phase transition takes place at the temperature at which the first change in the Mössbauer spectrum occurs and the peak temperature of the high-temperature phase transition is identical with the temperature where the Mössbauer

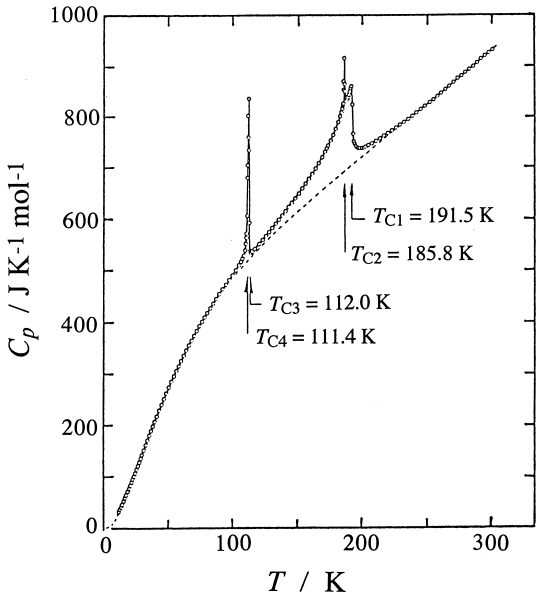

Fig. 27. Molar heat capacity of the mixed-valence complex $[Fe_3O(O_2CCH_3)_6(py)_3]\cdot(py)$. Broken curve indicates the normal heat capacity (Refs. 83 and 84).

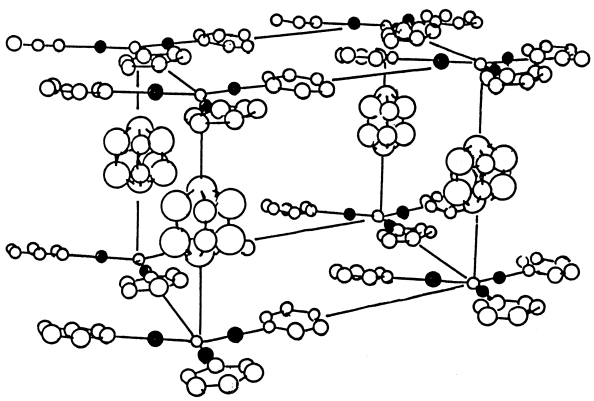

Fig. 28. Schematic drawing of the crystal structure of $[Fe_3O(O_2CCH_3)_6(py)_3]\cdot(py)$ (Ref. 73). The acetato ligands are not shown for clarity. Crystallographic C_3 axis runs through the central oxygen atoms of the Fe_3O complexes.

spectrum becomes a single average doublet. Moreover, the large temperature range involved in the high-temperature phase transition fully overlaps with the temperature region where the drastic change in the Mössbauer spectrum is occurring. Therefore, the observed phase transitions are concluded to arise from the intramolecular electron-transfer event in the mixed-valence complex. The entropy gain associated with the phase transitions is (30.6 ± 0.8) J K^{-1} mol^{-1}, as listed in Table 5 together with those for other complexes. Since the entropy due to the valence-detrapping is either R ln 3 (= 9.1 J K^{-1} mol^{-1}) or R ln 4 (= 11.5 J K^{-1} mol^{-1}) at most, the observed transition entropy obviously contains extra contributions other than the intramolecular electron-transfer.

A clue for the extra candidates lies behind its crystal structure. A schematic drawing of the molecular packing in the valence-detrapped high-temperature phase of $[Fe_3O(O_2CCH_3)_6(py)_3]\cdot(py)$ is shown in Fig. 28.[73] For simplicity, the acetato

Table 5. Entropy Gain at the Phase Transitions Observed in the Mixed-Valence Complexes with the Formula $[M^{III}_2M^{II}O(O_2CCH_3)_6L_3]\cdot(solv)$ (in the Unit of J K^{-1} mol^{-1})

	Complex				T_C/K	Entropy			
	M(III)	M(II)	L	solv		ΔS(metal)	ΔS(solvate)	ΔS(calcd)	ΔS(obsd)
1	Fe	Fe	py	py	112, 191	R ln 3	R ln 12	29.8	30.6 ± 0.8
8	Fe	Co	py	py	150	—	R ln 3	9.1	10.3
2	Mn	Mn	py	py	185	R ln 4	R ln 18	35.6	35.8
3	Fe	Fe	py	$CHCl_3$	208	R ln 4	R ln 8	28.8	28.1 ± 0.4
4	Fe	Fe	4-Me-py	$CHCl_3$	94	R ln 4	R ln 2	17.3	17.2 ± 1.4
5	Fe	Fe	3-Me-py	3-Me-py	282	R ln 3	R ln 2	14.9	13.7 ± 0.7
6	Fe	Fe	3-Me-py	toluene	293	R ln 3	R ln 2	14.9	15.1

ΔS(metal): Entropy gain due to conformational change of the M_3O complex. ΔS(solvate): Entropy gain due to orientational disordering of the solvate molecule. ΔS(cacld) = ΔS(metal) + ΔS(solvate).

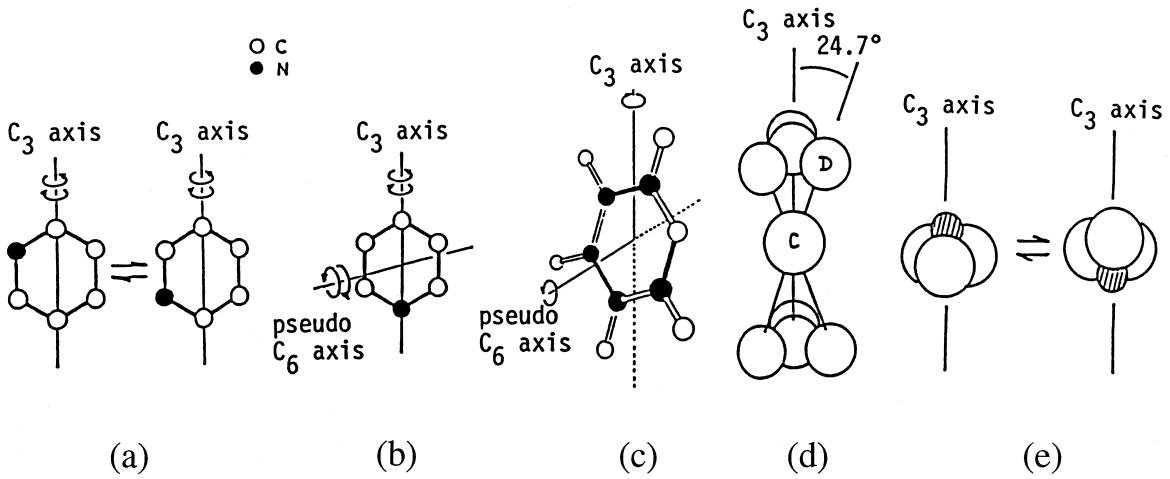

Fig. 29. Orientational disordering of the solvate molecules in the crystal lattice of the trinuclear complexes $[M_3O(O_2CCH_3)_6(L1)_3]\cdot(solvate)$, designating [M, L1, solvate] for short. (a) Pyridine in [Fe, py, py] (Ref. 73), (b) pyridine in $[Fe_2CoO(O_2CCH_3)_6(py)_3]\cdot(py)$ (Ref. 91), (c) pyridine in [Mn, py, py] (Ref. 85), (d) deuterated chloroform in [Fe, py, $CDCl_3$] (Ref. 86), and (e) chloroform in [Fe, 4-Me-py, $CDCl_3$] (Ref. 88).

ligands are not drawn. As described previously, the space group of this crystal is $R32$. Along the crystallographic C_3 axis, the metal complexes and pyridine solvate molecules occupy alternating sites of the 32 symmetry. That is, each pyridine solvate molecule is sandwiched between two metal complexes. The plane of the pyridine solvate molecule is perpendicular to the metal-complex plane. As required by the presence of the C_3 axes along which the metal complexes are stacked, the pyridine solvate molecules are disordered, with at least three orientational positions. On the other hand, solid-state ^{2}H NMR for the iron complex with deuterated pyridine solvate molecule studied by Hendrickson and his collaborators[73] revealed detailed molecular dynamics. As illustrated in Fig. 29a, the molecular plane of the pyridine jumps among three positions about the crystallographic C_3 axis. In each planar position, the pyridine solvate molecule librates among four positions, where in each of these positions two carbon atoms are on the C_3 axis. As the result, the pyridine solvate molecule converts from being static to dynamically interconverting among twelve different orientations.

Now that the dynamics of the solvate molecule has been clarified, the transition entropy can be interpreted as follows. If each metal complex converts from being statically distorted in one state to interconverting dynamically between three vibronic states when the complex is heated from low-temperatures, this contributes R ln 3 to the entropy gain. The sum of R ln 3 for the metal complex and R ln 12 for the pyridine solvate molecules is R ln 36 (= 29.8 J K^{-1} mol^{-1}). This value agrees well with the observed entropy gain (30.6 ± 0.8) J K^{-1} mol^{-1}. This fact provides a definitive evidence that the intramolecular electron transfer does proceed in cooperation with orientational disordering of the solvate molecule.

The phase transition behavior is drastically altered only by substitution of the central metal ions. Figure 30[82,85] represents molar heat capacity of $[Mn_3O(O_2CCH_3)_6(py)_3]\cdot(py)$. This complex brings about a sharp first-order phase transition at 184.7 K and the transition entropy amounts to ΔS = 35.8 J K^{-1} mol^{-1}, which is much greater than that of the homologous iron complex. Variable-temperature ^{2}H NMR study of the deuterated pyridine complex[85] revealed that each pyridine solvate molecule is rapidly reorienting about its local pseudo C_6 axis and, moreover, the pyridine plane jumps between three positions about the crystallographic C_3 axis, in each of which the pyridine plane is tipped off the C_3 axis by about 15° (see Fig. 29c).

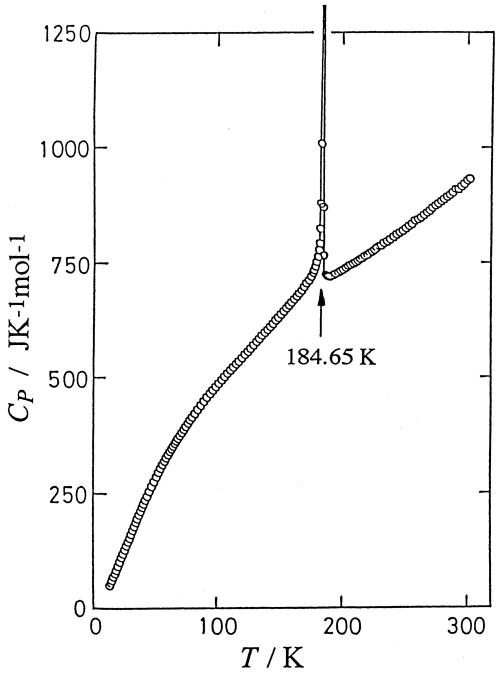

Fig. 30. Molar heat capacity of the mixed-valence complex $[Mn_2O(O_2CCH_3)_6(py)_3]\cdot(py)$ (Refs. 82 and 85).

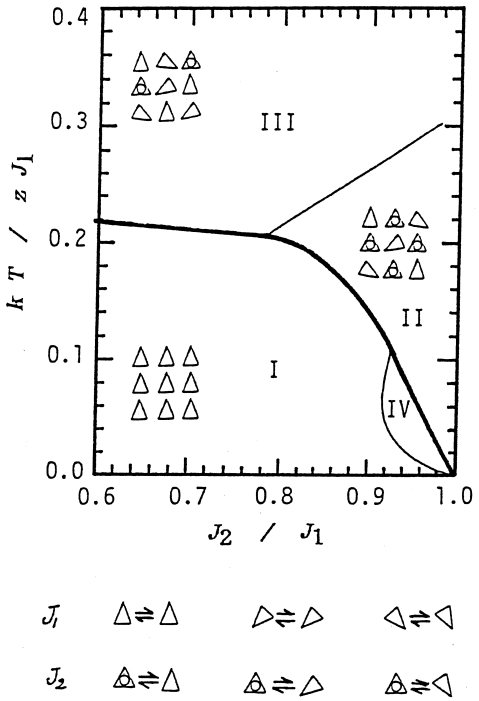

Fig. 31. Phase diagram calculated by Stratt and Adachi for the phase transitions in mixed-valence M_3O complexes that crystallize in the $R32$ space group. The vertical axis is temperature plotted in unit of J_1z/k, where k is the Boltzmann constant, z is the number of M_3O complexes surrounding each M_3O complex, and J_1 is the interaction energy of two neighboring complexes, both of which are distorted parallel to each other. The horizontal axis is the ratio of the "antiferromagnetic" (J_2) to the "ferromagnetic" (J_1) coupling, where J_2 is the interaction energy for two neighboring complexes, one of which is distorted and the other is undistorted. The phase boundaries of I–II, I–III, and IV–II correspond to a first-order phase transition while those of II–III and I–IV are of second-order (Ref. 93).

In this case, the expected entropy gain due to the solvate molecule would be R ln 18. If we assume that four minima on the adiabatic potential surface are established in the valence-detrapped high-temperature phase, its entropy gain is R ln 4. The sum of these two contributions (35.6 J K^{-1} mol^{-1}) agrees well with the observed value.

As evidenced by many instances (see Table 5), the intramolecular electron transfer occurs in these trinuclear mixed-valence complexes by coupling with the onset of orientational disordering of the solvate molecules. The intermolecular interactions responsible for such a coupling may be electric dipole–dipole interactions between the complex and the solvate molecules. Actually, when the solvate molecule is benzene having no electric dipole moment, the mixed-valence complex does not bring about a phase transition arising from the electron transfer. It should be remarked here that the onset of conformational change of solvate molecule is not necessarily a condition for intramolecular electron transfer. For example, although a crystal of mixed-valence complex $[Fe_3O(O_2CCH_2CN)_6(H_2O)_3]$ does not contain any solvent molecules, a phase transition due to valence-detrapping really occurs at 128 K.[92]

A simple but fundamental question arises here as to why only the $[Fe_3O(O_2CCH_3)_6(py)_3]\cdot(py)$ complex exhibits two phase transitions (a first-order phase transition at low temperature and a higher-order transition at high temperature) in contrast to a single first-order phase transitions in other complexes. The first statistical theoretical model to describe the phase transitions observed for mixed-valence Fe_3O complexes was proposed by Kambara et al.[81] Stratt and Adachi[93] took an imaginative and insightful approach. They assumed that the same type of intermolecular interactions exists between nearest neighbor complexes as were assumed by Kambara et al. Figure 31 shows the phase diagram calculated with this theory. J_1 and J_2 are parameters that gauge the pairwise intermolecular interaction where two neighboring M_3O complexes are distorted parallel to each other or only one is distorted, respectively. The "spin" type Hamiltonian of Stratt and Adachi leads logically to the idea of two interpenetrating sublattices of Fe_3O complexes. Each Fe_3O complex in sublattice A is surrounded by six Fe_3O complexes which are in sublattice B and vice versa. At low temperatures Fe_3O complexes in both sublattices are valence-trapped. Furthermore, the "sense of trapping" is oriented in the same direction for sublattices A and B. At about 112 K the complex makes a first-order phase transition from this "ferrodistortive" phase to a phase where one sublattice has valence trapped complexes and the sense of distortion is random. The other sublattice has an appreciable number of undistorted (delocalized) complexes with randomly oriented valence-trapped complexes. This "antiferrodistortive" phase exists in the 112–190 K region. At about 190 K there is a higher-order phase transition to the "paradistortive" phase where there is a random distribution of distorted and undistorted complexes due to the fact that all complexes are rapidly tunneling among the four minima on their adiabatic potential energy ground

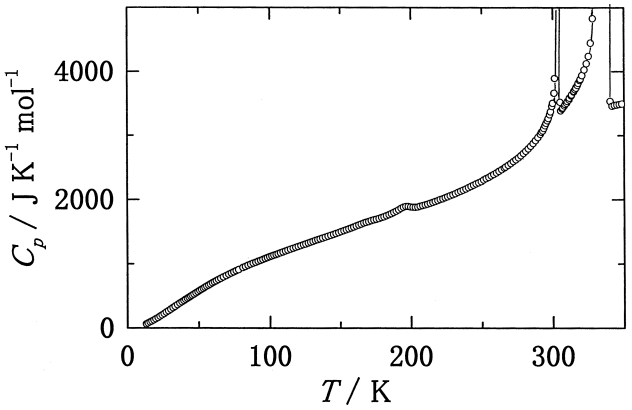

Fig. 32. Molar heat capacity of the mixed-valence complex $[Fe^{III}_2Fe^{II}O(O_2CC_{13}H_{27})_6(py)_3]$. The small anomaly around 200 K is related to the intramolecular electron transfer.

state surface. Their theoretical model suggests the existence of this type of double phase transitions in the range $0.8 < J_2/J_1 < 0.9$. When the interaction ratio J_2/J_1 is less than 0.8, only a single first-order phase transition can occur, as observed in many M_3O mixed-valence complexes. Although the theory by Stratt and Adachi ignores the effects of the solvate molecules, qualitative aspects inherent in the phase transitions occurring in the trinuclear mixed-valence complexes are well interpreted.

4.3 Phase Transitions in Trinuclear Mixed-Valence Complexes with long Alkyl Chains. In the mixed-valence complexes so far explained, $[M^{III}_2M^{II}O(O_2CC_nH_{2n+1})_6(L1)_3]\cdot$(solvate) with $n = 1$, the intramolecular charge (or electron) transfer always occurred in cooperation with the disordering of solvate molecules stoichiometrically amalgamated in the crystal lattice. However, this is not the case for the complexes having long alkyl chains in the acetato ligands.

^{57}Fe Mössbauer effect study[94] on the trinuclear iron mixed-valence complexes $[Fe^{III}_2Fe^{II}O(O_2CC_nH_{2n+1})_6(py)_3]$ (n = 13, 15, 17) revealed that intramolecular electron transfer occurs around 200 K. Figure 32 shows the molar heat capacity of the complex with $n = 13$. The large heat capacity anomalies appearing above 300 K correspond to structural phase transitions and fusion, which are independent of the charge transfer event. Since ^{57}Fe Mössbauer spectroscopy suggests an intramolecular electron transfer around 200 K, it is very likely that the small heat capacity anomaly observed around 200 K might be the phase transition due to the intramolecular electron transfer. Approximating the normal heat capacity curve by a cubic polynomial of temperature, one could separate the excess heat capacity due to the phase transition from the observed values. As shown in Fig. 33a by solid circles, the excess heat capacity consists of two peaks centered at 170 K and 195 K, in spite of a single batch preparation. These two anomalies were reproduced by the once-melted specimen (open circles in Fig. 33a). The entropy gains are ΔS = 12.8 J K^{-1} mol^{-1} for the as-prepared sample and 14.3 J K^{-1} mol^{-1} for the once-melted specimen (see Fig. 33b). As described in section 4.1, the entropy expected from the adiabatic potential energy surface would be either R ln 3 (= 9.13 J K^{-1} mol^{-1}) or R ln 4 (= 11.53 J K^{-1} mol^{-1}) at most. As the observed entropy gains are fairly large in comparison with the theoretical values, one of the two

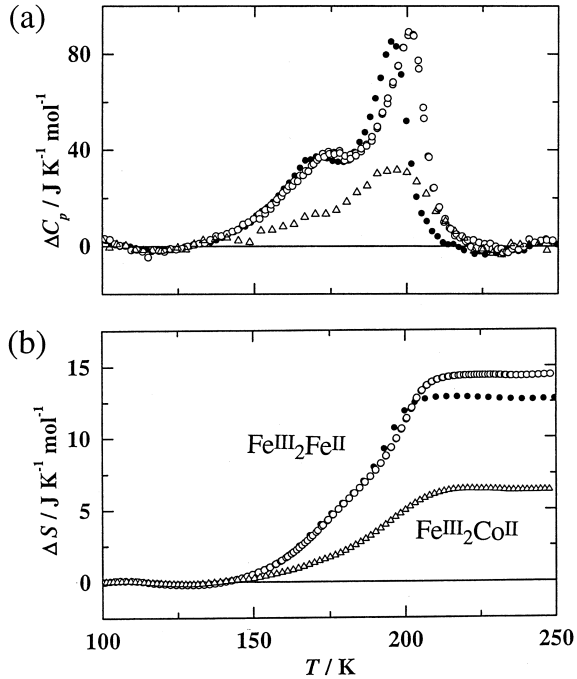

Fig. 33. (a) Excess heat capacities and (b) entropy gains due to the anomalies around 200 K for $[Fe^{III}_2Fe^{II}O(O_2CC_{13}H_{27})_6(py)]$ and $[Fe^{III}_2Co^{II}O(O_2CC_{13}H_{27})_6(py)]$. Closed and open circles indicate the as-prepared and once-melted samples of the Fe_3O-complex while open triangles are the as-prepared sample of Fe_2CoO-complex (Refs. 96 and 97).

anomalies might be due to a different origin than the electron transfer.

In order to examine this possibility, we measured the heat capacity of an isostructural non-mixed-valence complex in which divalent iron ion is replaced by cobalt ion $[Fe_2CoO(O_2CC_{13}H_{27})_6(py)_3]$. As expected, its heat capacity exhibited a very broad heat capacity anomaly in the same temperature region as the mixed-valence complex. The excess heat capacity and the entropy gain (6.4 J K^{-1} mol^{-1}) are compared with those of the mixed-valence complex in Figs. 33a and b, respectively. Although the cause responsible for this anomaly is not clear at present, it is obvious that this anomaly has no relation to the charge transfer, because the cobalt complex does not belong to a mixed-valence system. At any rate, we can safely conclude that the mixed-valence iron complex exhibits two kinds of phase transitions in the 130–220 K temperature range: one is due to the charge transfer and the other is not. As the shape of the heat capacity anomaly at low temperature side bears close resemblance to that of the cobalt complex, it is very likely that the sharp anomaly appearing at higher temperature side would arise from the intramolecular electron transfer event.

If we assume that the entropy change due to the non-electron origin of the mixed-valence complex is identical with that of the non-mixed-valence complex, the entropy gain due to the intramolecular electron transfer should be the difference between the transition entropies for the two complexes. That amounts to (6.4–7.9) J K^{-1} mol^{-1}. If one takes into account the ambiguity involved in the estimate of the normal heat ca-

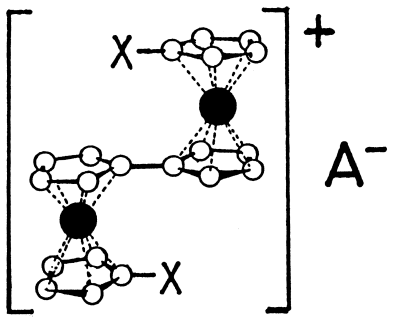

Fig. 34. Schematic drawing of molecular structure of mixed-valence 1′,1‴-disubstituted biferrocenium cation (X: substituent, A: anion such as I_3, PF_6, SbF_6).

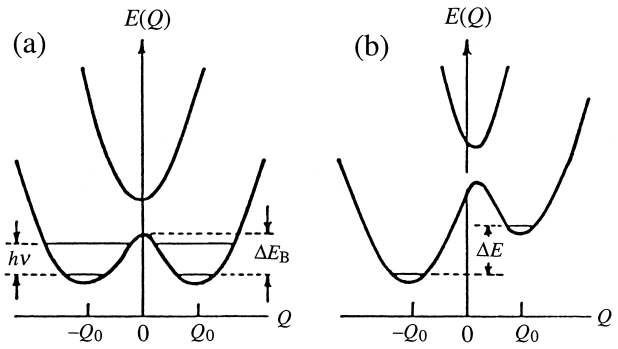

Fig. 35. Potential energy surface $E(\theta)$ drawn as a function of the out-of-phase combination ($Q = Q_A - Q_B$) of the two symmetric metal-ligand breathing vibrational modes (Q_A and Q_B) of the two halves of a binuclear mixed-valence species. (a) for a symmetric mixed-valence complex in the absense of environmental effects. (b) for results if the environment about the binuclear mixed-valence complex is asymmetric (Refs. 77 and 100).

pacity curves, this entropy gain can be approximated by R ln 3 = 9.1 J K^{-1} mol^{-1}. That is to say, the number of minima in the adiabatic potential surface would be three for this complex. In the crystal of this complex, it is anticipated that the long alkyl chains and the metal cores form an alternative stacking layer structure. The elastic thick layers of alkyl chains seem to absorb the strain produced by dynamic distortions of the trinuclear metal core due to intramolecular electron transfer. This is probably a reason why the intramolecular electron-transfer occurs without help of any solvent molecules.

4.4 Electron Transfer in Binuclear Mixed-Valence Complexes. In this section we shall describe calorimetric studies mainly on the salts of mixed-valence 1′,1‴-disubstituted biferrocenium(+1) cations shown in Fig. 34. Electron transfer in mixed-valence molecular systems is generally described by the PKS model[98] based on a vibronic approach. As mixed-valence complexes are electronically labile, the lowest energy electronic states are vibronic and as a result the complexes are very sensitive to their environments.[99] In the absence of environmental effects, a binuclear $Fe^{II}Fe^{III}$ mixed-valence complex has two electronic states which would be electronically degenerate. The two potential energy curves would be superimposed and strong vibronic coupling would result. Certain vibrational coordinates, such as the out-of-phase combination of the totally symmetric ring-metal-ring breathing modes on each metallocene moiety in Fig. 34, would couple to the two electronic states. Two energetically degenerate vibronic states result, for which the two parabolic potential-energy curves are displaced relative to each other in the nuclear coordinate space Q_0 of the coupled vibrational mode.[77,100] If these two vibronic states interact, one can expect an adiabatic potential shown in Fig. 35a.[100] The ground state surface has two minima, both at the same energy. In general there will be several vibrational energy levels below the barrier height ΔE_B. In Fig. 35a only the zeroth vibrational level and one fundamental at $h\nu$ are shown, where h is the Planck constant and ν is the vibrational frequency.

For a binuclear $Fe^{II}Fe^{III}$ complex in an asymmetric environment, just as in the solid state, the potential energy diagram is as shown in Fig. 35b. The two vibronic states are not at the same energy. There is an energy difference ΔE between the two states. This difference reflects the different environments near the two iron ions in the binuclear complex. The $Fe_a^{II}Fe_b^{III}$ vibronic state is stabilized relative to the $Fe_a^{III}Fe_b^{II}$ vibronic state. When the thermal energy kT is less than ΔE, the complex is found in the $Fe_a^{II}Fe_b^{III}$ state. If the complex is to convert from $Fe_a^{II}Fe_b^{III}$ to $Fe_a^{III}Fe_b^{II}$, it needs to be thermally excited by ΔE or more. Since there will be many vibrational levels on both sides of the asymmetric double well, it can then tunnel from a "left" vibrational level to a vibrational level on the "right" side.

Vibronic coupling works efficiently to make a small polaron migrate over the metal centers within a complex molecule. Those compounds possess a potential of charge ordering in their crystalline phases at low temperatures.[101,102] Transitions between such a valence-trapped and a valence-detrapped state have been observed by Mössbauer spectroscopy in some binuclear complexes. Non-substituted biferrocenium(+1) triiodide[103] and many dialkylbiferrocenium triiodids[104,105] are known to bring about a transition from a valence-trapped to a valence-detrapped state above 200 K.

We measured heat capacities of four biferrocenium salts. 1′,1‴-Diiodobiferrocenium(+1) hexafluoroantimonate[106] really gave rise to a phase transition arising from the valence-detrapping at 134 K. The entropy gain (6.0 ± 0.5) J K^{-1} mol^{-1} is very close to R ln 2 (= 5.76 J K^{-1} mol^{-1}), the value expected for two energetically equal vibronic states as shown in Fig. 35a. In contrast to this, biferrocenium(+1) triiodide[107] and 1′,1‴-diethylbiferrocenium(1) triiodide[108] bring about very small heat capacity anomalies at 328 K and 250 K, respectively. As summarized in Table 6, the entropy gains are only (1.77 ± 0.06) and 1.0 J K^{-1} mol^{-1}, much lower than R ln 2. This fact may imply an incomplete valence-detrapping state at high temperatures. In other word, the environment in the crystal lattice is asymmetric even above the phase transition temperature and hence the energy difference ΔE between the two ground vibronic states in Fig. 35b will not be zero but will remain at a finite value. The temperature variation of ΔE is schematically illustrated in Fig. 36 for the two cases in a framework of a mean-field approximation.

Interestingly, when the substituent X in Fig. 34 is Br or I and A is I_3, the 1′,1‴-disubstituted-biferrocenium(+1) triio-

Table 6. The Enthalpy and Entropy Gains due to Phase Transition or Heat Capacity Anomaly in the Mixed-Valence 1′,1‴-Disubstituted Biferrocenium Salts, $[(C_5H_4XFe)_2(C_{10}H_8)]^+A^-$

Compound		T	ΔH	ΔS	Remarks[a)]
X	A	K	J mol^{-1}	J K^{-1} mol^{-1}	
H	I_3	328	538 ± 37	1.77 ± 0.06	(CO) $\Delta E/hc = 700$ cm^{-1}
I	I_3	0.6		R ln 2	(MQP) $\delta/hc = 1.0$ cm^{-1}
I	SbF_6	134	740 ± 50	6.0 ± 0.5	(CO) $\Delta E/hc = 0$
C_2H_5–	I_3	250		1.0	(CO) $\Delta E/hc = 750$ cm^{-1}

a) CO: charge ordering at low temperatures, MQP: molecular quantum paraelectrics, ΔE: energy difference between the two vibronic states at the phase transition temperature, δ: tunnel splitting, h: Planck's constant, c: velocity of light.

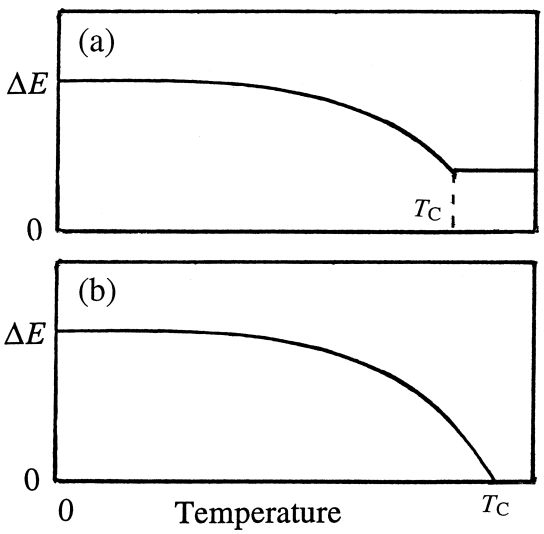

Fig. 36. Schematic drawing of temperature dependence of the energy difference ΔE between two ground vibronic states shown in Fig. 35b. In the case of (a), ΔE remains finite owing to an asymmetric environmental effect above the phase transition temperatureT_C while (b) corresponds to the case in which the two ground energy levels become equal.

dides remain in a valence-detrapped state even at 4.2 K.[109,110] Structural analysis for 1′,1‴-diiodobiferrocenium(+1) triiodide (hereafter, $I_2Fe_2{}^+I_3{}^-$ for short)[111] revealed that two iron atoms in a cation are related to each other by a symmetry center and thus are equivalent at room temperature (Fig. 37). This fact means that $I_2Fe_2{}^+I_3{}^-$ is in the valence-detrapped state at room temperature. Even at 4.2 K, the two iron atoms in the cation remain equivalent, because only one quadruple-split doublet was observed by ^{57}Fe Mössbauer spectroscopy and EPR measurements at 4.2 K gave a relatively isotropic g tensor characteristic of a valence-detrapped state.[109] It is noted, however, that the valence-detrapped phase should be interpreted not as a statically electron-delocalized state (i.e. single-minimum potential) but as a dynamically disordered state, because IR spectroscopy shows the existence of a potential barrier separating two valence-trapped configurations of the cation.[111]

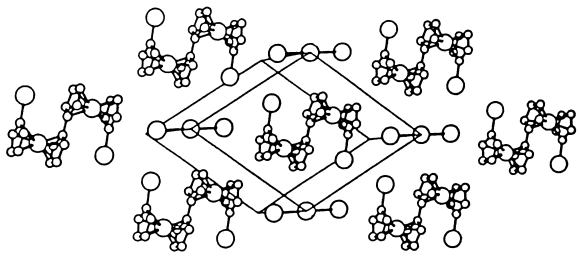

Fig. 37. Crystal structure of 1′,1‴-diiodobiferrocenium triiodide. There are alternating stacks of cations and anions (Ref. 111).

These two configurations are, therefore, degenerate at high temperatures and contribute R ln 2 to the entropy.

In order to elucidate how this entropy is removed at low temperatures, say below 4.2 K, following the requirement of the third law of thermodynamics, we measured the heat capacity of $I_2Fe_2{}^+I_3{}^-$ complex by adiabatic calorimetry between 80 mK and 25 K.[112] One of two ways might be anticipated: either a phase transition or none. If a phase transition occurs, this complex would have a charge-ordered ground state similar to those in other biferrocenium salts.[106–108] On the other hand, if no phase transitions take place, a quantum-mechanical tunneling would be incorporated into the double-minimum adiabatic potential so as to lift the degeneracy without long-range order. The observed heat capacity of the $I_2Fe_2{}^+I_3{}^-$ complex is shown in Fig. 38 on a logarithmic scale. Open circles plotted below 2 K correspond to a pellet sample, while solid circles between 1 K and 25 K are for a powder sample. A discrepancy detected between the two sets of data is based on a result in the pellet sample.[112] Two heat capacity anomalies were found: one takes place below ca. 0.2 K and the other is a broad peak centered around 0.6 K. The former arises from a magnetic interaction between the paramagnetic cations. The anomaly occurring around 0.6 K is obviously a Schottky-type heat capacity corresponding to a thermal excitation between two energy levels. The solid curve in Fig. 38 corresponds to a two-level Schottky heat capacity with an energy difference of $\delta/hc = 1$ cm^{-1}, where c is the velocity of light. The presence of the Schottky heat capacity anomaly demonstrates the existence of a double-well potential; there is a tunnel splitting between the vibronic

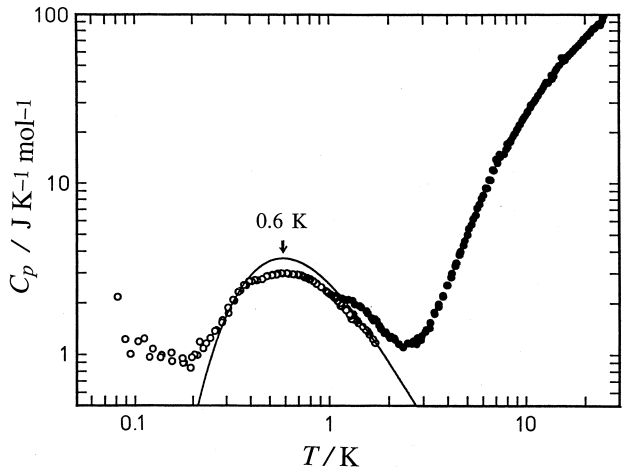

Fig. 38. Molar heat capacity of the mixed-valence complex 1′,1‴-diiodobiferrocenium triiodide. The solid curve shows the two-energy-level Schottky anomaly with δ/hc = 1 cm^{-1} (Ref. 112).

ground states and hence a charge-ordering phase transition in $I_2Fe_2^+I_3^-$ is absent. This type of nuclear tunneling has been expected to exist in the mixed-valence systems both from experiment[107] and from a theoretical treatment by Kambara et al.[100,113] However, it is indeed in this complex that the nuclear tunneling was actually and directly observed for the first time. In the sense that the quantum effect prevents the charge ordering with ferroelectric long-range order, the $I_2Fe_2^+I_3^-$ complex is regarded as a molecular quantum paraelectric. In fact, a Curie-like behavior characteristic of a paraelectric was observed in a preliminary dielectric measurement with the 0.4–20 kHz frequency range between 4 and 300 K.[112]

4.5 Halogen-Bridged MMX-type Mixed-Valence Complex. One-dimensional substances have been known to exhibit unique electronic, magnetic, and optical properties. In particular, halogen-bridged MMX-type one-dimensional mixed-valence complexes have drawn great attention because they have potentially the following four electronic states:

$$\cdots X^- – M^{2.5+} – M^{2.5+} – X^- – M^{2.5+} – M^{2.5+} – X^- – M^{2.5+} – M^{2.5+} – X^- \cdots \quad \text{(A)}$$

$$\cdots X^- — M^{2+} – M^{2+} — X^- – M^{3+} – M^{3+} – X^- — M^{2+} – M^{2+} — X^- – M^{3+} – M^{3+} – X^- \cdots \quad \text{(B)}$$

$$\cdots X^- — M^{2+} – M^{3+} – X^- — M^{2+} – M^{3+} – X^- — M^{2+} – M^{3+} – X^- — M^{2+} – M^{3+} – X^- \cdots \quad \text{(C)}$$

$$\cdots X^- — M^{2+} – M^{3+} – X^- – M^{3+} – M^{2+} — X^- — M^{2+} – M^{3+} – X^- – M^{3+} – M^{2+} — X^- \cdots \quad \text{(D)}$$

Mode (A) is an averaged-valence state and has the possibility of either a Mott-Hubbard insulator or a one-dimensional metal. Mode (B) is a mixed-valence insulating state (CDW). Modes (C) and (D) are a charge-polarization state and an alternate-charge-polarization state, respectively. As an unpaired electron exists in the (–M^{2+}–M^{3+}–) unit, modes (C) and (D) are anticipated to be paramagnetic. Since no cell doubling occurs in the case of mode (C), either a Mott–Hubbard insulator or a one-dimensional metal is expected. On the other hand, mode (D) is expected to be an insulator analogous to a spin-Peierls state.

Two main families of the MMX-chain complexes have so far been reported: $M_4[Pt_2(pop)_4X_4]\cdot nH_2O$ (M = Li, K, Cs, NH_4; pop = diphosphonato, $P_2H_2O_5^{2-}$; X = Cl, Br, I) and $M_2(dta)_4I$ (M = Ni, Pt; dta = dithioacetato, $CH_3CS_2^-$). Interestingly, electrical conductivity and thermoelectric power measurements for a single crystal of $Pt_2(dta)_4I$ parallel to the chain axis *b* revealed that this complex exhibits a metallic temperature dependence above a metal–semiconductor transition temperature T_{M-S} = 300 K.[114–117] A metallic behavior was first observed in $Pt_2(dta)_4I$ among halogen-bridged one-dimensional transition-metal complexes. This metal–semiconductor transition was also confirmed by magnetic susceptibility measurement for a polycrystalline sample.[116,117] Furthermore, temperature dependence of the electrical conductivity and thermoelectric power measurements showed a first-order phase transition around 360 K. From single-crystal X-ray structure analyses,[114,115,118] it was revealed that a first-order phase transition occurs at T_{trs} = 365 K from the low-temperature phase with space group *C*2/*c* to the high-temperature phase with *A*2/*m*, in which the cell volume is a half of that of the low-temperature phase. This phase transition is of the order-disorder type concerning conformational change of the dta-ligands (see Fig. 39).[118]

Moreover, the magnetic susceptibility shows a convexity at 90 K, which suggests the existence of a phase transition.[116,117] From variable-temperature infrared and polarized Raman spectroscopies at room temperature and ^{129}I Mössbauer spectroscopy[116,117] at 16 and 80 K, together with the experimental results mentioned above, it is expected that the $Pt_2(dta)_4I$ complex is in a one-dimensional metallic phase with mode (A) above T_{M-S} = 300 K, in a semiconducting phase with mode (C) between 90 and 300 K, and in an insulating phase with mode (D) below 90 K.

In order to elucidate the relationship between various phases, heat capacity measurements were made for a powder sam-

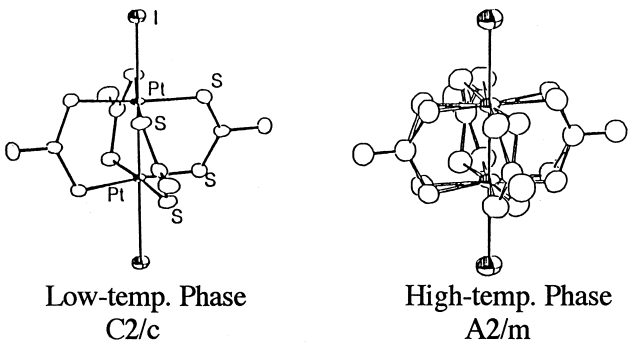

Fig. 39. A part of one-dimensional arrangement of the halogen-bridged mixed-valence complex, $Pt_2(dta)_4I$. In the high-temperature phase, two conformational disorders of each dta-ligand are drawn with equal probability (Ref. 118).

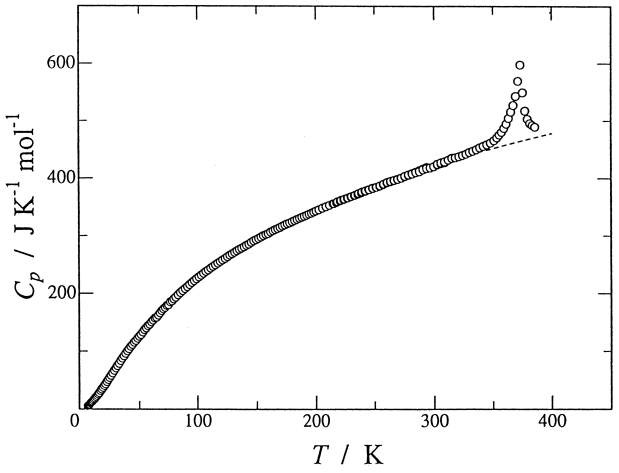

Fig. 40. Molar heat capacity of $Pt_2(dta)_4I$. The broken curve implies normal heat capacity (Ref. 119).

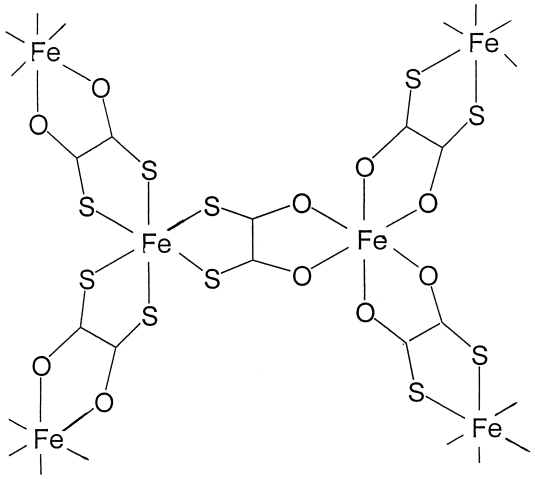

Fig. 41. Schematic drawing of the dto-bridged network structure in $\{(n\text{-}C_3H_7)_4N[Fe^{II}Fe^{III}(dto)_3]\}_\infty$ (Ref. 121).

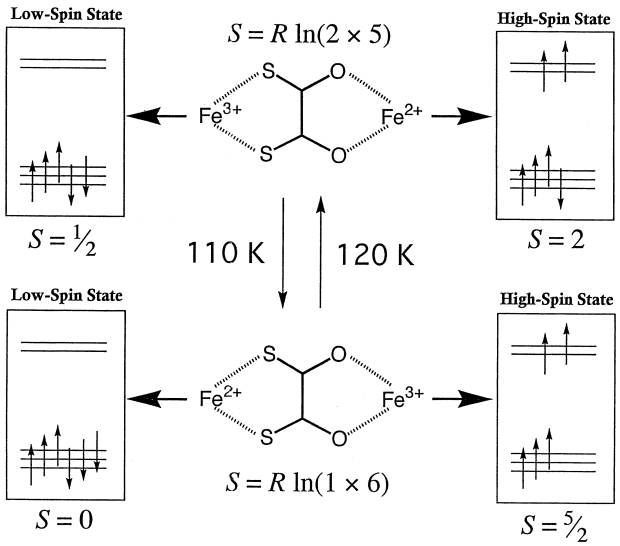

Fig. 42. Schematic representation of the spin-state conversion due to electron transfer phenomenon in $\{(n\text{-}C_3H_7)_4N[Fe^{II}Fe^{III}(dto)_3]\}_\infty$. It should be remarked that symbol S has been used both for the spin quantum number and for the entropy due to the spin multiplicity (Ref. 121).

ple of this complex. Molar heat capacities of the $Pt_2(dta)_4I$ crystal are plotted in Fig. 40.[119] A heat capacity peak due to a phase transition was observed at T_{trs} = 373.4 K. The total enthalpy and entropy gains due to the phase transition were ΔH = (1.91 ± 0.02) kJ mol^{-1} and ΔS = (5.25 ± 0.07) J K^{-1} mol^{-1}, respectively. The transition entropy is close to R ln 2 (= 5.76 J K^{-1} mol^{-1}). If the four dta-ligands bridging two metal ions independently reorient between two directions in the high-temperature phase, the transition entropy amounts to $4R$ ln 2 (= 23.1 J K^{-1} mol^{-1}). However, this is not the case. The fact that the experimental value of the transition entropy is well approximated by R ln 2 suggests that the reorientational motions of the four dta ligands would not be independent but should be synchronized.

As described above, various experiments so far reported have suggested the metal-semiconductor transition at $T_{M\text{–}S}$ = 300 K, corresponding to a Mott transition from one-dimensional metallic phase with mode (A) to semiconducting phase with mode (C), and a spin-Peierls-like phase transition with mode (D) below 90 K. However, the present calorimetric results did not give rise to any thermal anomalies at 90 K and 300 K. We performed heat capacity measurements for a single crystal of $Pt_2(dta)_4I$ in the 15–317 K range by ac calorimetry at 2 Hz. However, no thermal anomaly was detected around 90 K and 300 K. In general the change of a crystal lattice involved in a Mott transition is extremely small. Therefore the thermal anomaly due to the Mott transition at 300 K, if any, is too small to be detected by these calorimetries. On the other hand, since a Peierls or spin-Peierls transition gives rise to a change of crystal lattice due to dimerization, a thermal anomaly would be observed at 90 K if the transition actually occurs. In the case of a $Pt_2(dta)_4I$ crystal, however, as the spin in the crystal is still alive below 90 K, the change in the lattice would be very small. This might be the reason for our failure to observe a thermal anomaly at 90 K.

5. Spin State Conversion due to Charge-Transfer in the Mixed-Valence Iron Complex, $\{(n\text{-}C_3H_7)_4N[Fe^{II}Fe^{III}(dto)_3]\}_\infty$ (dto = $C_2O_2S_2$)

Recently a novel mixed-valence iron complex $\{(n\text{-}C_3H_7)_4N[Fe^{II}Fe^{III}(dto)_3]\}_\infty$ containing asymmetric ligand dto^{2-} (dithiooxalato: $C_2O_2S_2^{2-}$) was synthesized by Kojima and his coworkers.[120] As schematically drawn in Fig. 41,[121] two kinds of iron ions are anticipated to be octahedrally coordinated by six O atoms, $[FeO_6]$, and six S atoms, $[FeS_6]$, from the analogy of similar oxalato complexes.[122,123] Since the ligand field at the $[FeS_6]$ site is much stronger than that at the $[FeO_6]$ site, the iron ion surrounded by sulfur atoms is characterized by low-spin state, while that surrounded by oxygen atoms shows high-spin state. As shown in Fig. 42,[121] at room temperature iron ions sitting in the $[FeS_6]$ site are low-spin Fe(III) with spin quantum number S = 1/2, while those of the $[FeO_6]$ site are high-spin Fe(II) with S = 2. When the temperature is decreased, electron transfer occurs from the $[FeO_6]$ site to the $[FeS_6]$ site around 110 K and their oxidation states are inter-

changed. As the results, iron ions at the [FeO_6] site become high-spin Fe(III) with $S = 5/2$ and those at the [FeS_6] site are low-spin Fe(II) with $S = 0$. On the other hand, when the temperature of crystal is increased, the electron is reversely transferred around 120 K. Since the spin-state conversion takes place in the whole [FeO_6][FeS_6] system by the electron transfer, this phenomenon seems to be, at first glance, spin crossover. However, this is not the case, because the spin state at a given site always remains either HS- or LS-state when the electron transfer occurs. Although a great many spin crossover systems and mixed-valence systems have been identified, a conjugated system like the present complex has not been reported so far. Moreover, this complex exhibits ferromagnetic order below 6 K.

In order to throw light on this novel system from a thermodynamic viewpoint, we measured its heat capacity over a wide temperature region.[124] The molar heat capacities at temperatures below 300 K are plotted in Fig. 43.[124] A sharp peak and a broad heat capacity anomaly were observed at 122.4 K and 253.5 K, respectively. The heat capacity anomaly at 253.5 K can be attributed to the order-disorder type of phase transition due to conformational change in $(n\text{-}C_3H_7)_4N^+$ cation, judging from the fact that similar heat capacity anomalies have also been observed in some analogous molecule-based magnets such as $\{(n\text{-}C_4H_9)_4N[M^{II}Fe^{III}(ox)_3]\}_n$, where M = Fe or Zn.[125] The anomaly at 122.4 K obviously arises from the electron transfer phenomenon, because the transition temperature agrees well with the temperature where the anomaly is observed in the magnetic susceptibility.[121] Although the phase transition at 122.4 K does not occur isothermally, this should be regarded as a first-order phase transition because supercooling has been observed.

To determine the enthalpy and entropy gains due to the electron transfer phenomenon, a normal heat capacity curve was estimated by assuming a polynomial function of temperature, $aT^2 + bT + c$, over the 80–160 K range. By integrating excess

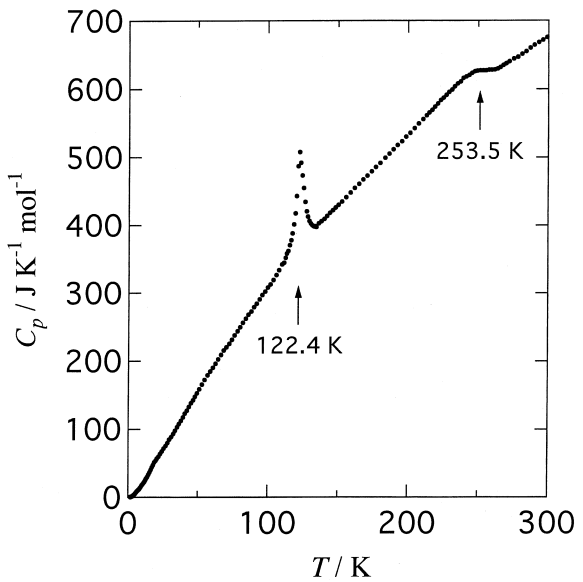

Fig. 43. Molar heat capacity of the mixed-valence complex $\{(n\text{-}C_3H_7)_4N[Fe^{II}Fe^{III}(dto)_3]\}_\infty$ (Ref. 124).

heat capacities beyond the normal heat capacity curve, we got $\Delta H = 1.04$ kJ mol^{-1} and $\Delta S = 9.20$ J K^{-1} mol^{-1}. The entropy change is larger than the spin-only value expected for the change in the spin multiplicity R ln(10/6) = 4.25 J K^{-1} mol^{-1}. As far as the ligand-field symmetry remains O_h through the phase transition, change in the orbital angular momentum contributes R ln[(3 × 3)/(1 × 1)] = 18.27 J K^{-1} mol^{-1} to the entropy gain. If this is the case, the total entropy gain due to spin and orbital amounts to 22.51 J K^{-1} mol^{-1}. However this is not the case, because this value is far beyond the experimental entropy. It should be remarked here that the orbital degeneracy such as $^5T_{2g}$ and $^2T_{2g}$ encountered in high spin Fe(II) and low spin Fe(III) in an O_h symmetry is usually lifted by the Jahn–Teller distortion to give a non-degenerate or lower-degenerate ground state. In such a case, the orbital contribution to the entropy becomes small or negligible. In the present complex, it is very likely that a trigonal distortion is encountered in the FeO_6 and FeS_6 sites. Under such situation, the ground terms $^5T_{2g}$ of Fe^{II}(HS) and $^2T_{2g}$ of Fe^{III}(LS) in O_h ligand-field symmetry are reduced to ^5E and ^2A in a trigonal symmetry, respectively. If this orbital contribution is fully taken into account, the electronic entropy gain due to spin and orbital will be R ln [(10 × 2)/6] = 10.01 J K^{-1} mol^{-1}. This value is very close to the experimental value of 9.20 J K^{-1} mol^{-1} due to the electron transfer phenomenon. Although we discussed the orbital contribution to entropy for octahedral and trigonal ligand-fields, there is a possibility that the actual ligand-field symmetry of the present complex is lower than trigonal symmetry. In such a case, the orbital contribution to the entropy gain is further reduced. Therefore, it may be concluded that the entropy gain expected from electron is in the range between R ln (10/6) = 4.25 J K^{-1} mol^{-1} due to the spin multiplicity and R ln (20/6) = 10.01 J K^{-1} mol^{-1} due to the spin and the orbital in trigonal symmetry.

At any rate, since the observed entropy gain is 9.20 J K^{-1} mol^{-1}, the entropy originating in intramolecular vibrations is considerably small in comparison to normal spin crossover phenomena. For example, about 35 J K^{-1} mol^{-1} was estimated for the vibrational contribution to the entropy change in the spin crossover phenomenon observed in $[Fe^{II}(NCS)_2(phen)_2]$[24] and 27 J K^{-1} mol^{-1} for $[Fe^{III}(3MeO\text{-}salenEt)_2]PF_6$.[56] The magnitude of vibrational entropy crucially depends on the bond lengths between metal ion and ligands. The longer the bond length, the greater the vibrational entropy is. The metal-ligand bond length is affected by the spin state of the metal ion: it is longer for HS-state than for LS-state. Therefore, the normal spin crossover phenomenon always involves a large entropy gain from the metal-ligand skeletal vibrations. Contrary to this, in the present complex, the oxidation state of each iron ion changes at a given site but the spin state is not altered. This is the reason for the very small entropy gain from the skeletal vibrational modes.

The present mixed-valence complex surely provides an interesting system, in which the spin state of the whole system dramatically changes by virtue of the electron transfer. At first glance, this phenomenon seems to be a kind of spin crossover phenomenon. However, the present calorimetric study clearly revealed that this novel phenomenon is quite different from usual (or classical) spin crossover phenomenon. From a view-

point of functionality the present material is expected to have a great potentiality.

6. Neutral-Ionic Phase Transition in TTF·CA

Organic charge-transfer crystals composed of electron-donor (D) and acceptor (A) molecules with 1:1 ratio are classified into two types. One is a group in which D and A molecules are separately stacked and the other is a group of alternate stacks or mixed stack. The former is usually a conductor or occasionally a superconductor, whereas the latter is always an insulator or a semiconductor. When the degree of charge transfer ρ is low, say $\rho < 0.5$, the complex is designated as quasi-neutral. On the other hand, the complex is regarded as quasi-ionic when $\rho > 0.5$. Some of the alternately stacked complexes undergo the so-called neutral-to-ionic (NI) transition associated with a change in the degree of ionicity ρ. This electron-induced phase transition is generally observed at high pressure but in exceptional cases it happens at ambient pressure.

The charge-transfer complex formed between tetrathiafulvalene and *p*-chloranil (TTF–CA: see Fig. 44)[126] had been the only complex which exhibits a temperature-induced NI transition at ambient pressure until other candidates (TMB–TCNQ),[127] (DMTTF–CA),[128] and (ClMePD–DMeDCNQI)[129] were discovered. The NI-transition in TTF–CA crystal takes place around 80 K.[126] According to optical spectra, its degree of charge transfer at atmospheric pressure is $\rho \approx 0.3$ in the high-temperature neutral phase, while it is $\rho \approx 0.7$ in the low-temperature ionic phase.[130,131] Spectroscopic measurements[132,133] showed the existence of "dimeric" distortion (–D-A–D-A–...) in the ionic phase and the NI-transition was found to be of first-order.[134] Moreover, some crystal polymorphs are known to be obtainable by different methods of synthesis.[131,134]

We measured heat capacities of different polymorphs of protonated TTFh_4–CA prepared by solution method as well as well-grown TTFh_4–CA and deuterated TTFd_4–CA crystals obtained by co-sublimation method.[135,136] Figure 45 demonstrates the molar heat capacity of TTFh_4–CA.[135] A very sharp heat-capacity peak due to the NI-transition was found at 82.5 K. As listed in Table 7, the enthalpy and entropy gains were $\Delta H = (504 \pm 5)$ J mol^{-1} and $\Delta S = (6.12 \pm 0.06)$ J K^{-1} mol^{-1}. Judging from the transition entropy, which is very close to R ln 2 (= 5.76 J K^{-1} mol^{-1}), one may conclude that the NI-transition is not of displacement-type but of order-disorder type. However, no such disorder has been found in TTF–CA crystals from X-ray (see Fig. 46)[137] and neutron[138] diffraction studies. Therefore, a plausible explanation for the origin of this large entropy change is softening of the acoustic lattice vibrations on going from the low-temperature ionic phase to the high-temperature neutral phase, namely, the variation of lattice vibrations probably by "dimerization" of the TTF and CA molecules.

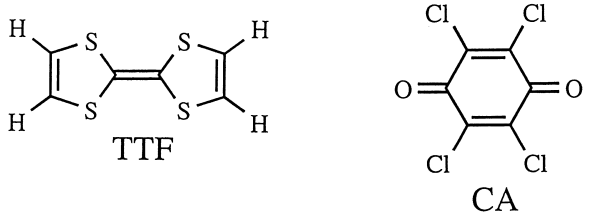

Fig. 44. Molecular structure of TTF and CA.

Table 7. Thermodynamic Quantities Associate with the NI-Transition in TTFh_4–CA and TTFd_4–CA Crystals Prepared by Co-sublimation Method (Ref. 135–137)

Complex	T_{NI}/K	ΔH/J mol^{-1}	ΔS/J K^{-1} mol^{-1}
TTFh_4–CA	82.5	504 ± 5	6.12 ± 0.06
TTFd_4–CA	86.4	496 ± 1	5.73 ± 0.02

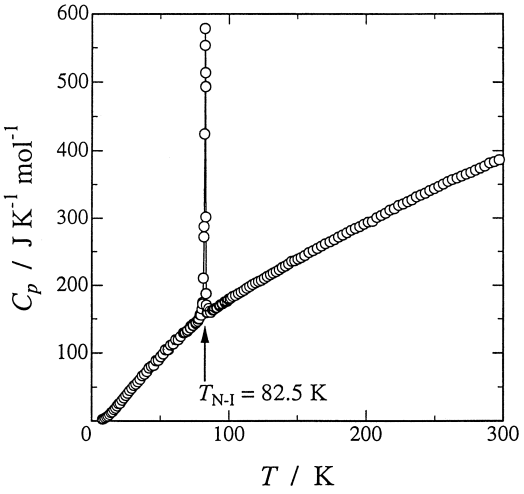

Fig. 45. Molar heat capacity of the charge transfer complex TTFh_4–CA (Ref. 135).

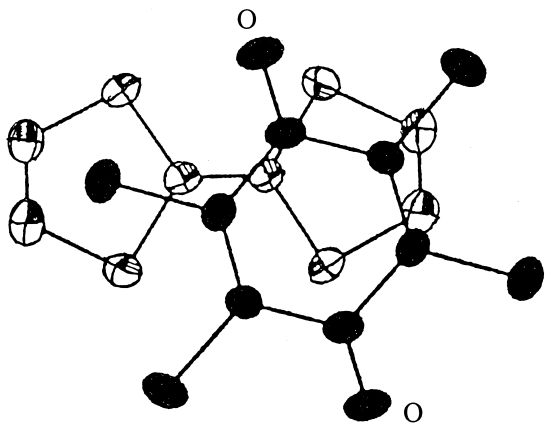

Fig. 46. Projection of the CA moiety onto the plane of the TTF moiety in TTF–CA (Ref. 137).

To confirm the validity of this interpretation, we measured the heat capacity of TTFd_4–CA crystals.[136] As listed in Table 7, the NI-transition was shifted by 3.9 K to the higher temperature side, while the entropy change (5.73 ± 0.02) J K^{-1} mol^{-1} was essentially the same as that for TTFh_4–CA. The shift of the NI-transition temperature seems to be rather large, since the mass difference between TTFd_4–CA and TTFh_4–CA is only 0.9 per cent. Therefore, this remarkable deuteration effect would be related to the weak hydrogen bonding [C–

H(D)···O and C–H(D)···Cl] anticipated between TTF and CA molecules. Since the unit axes b and c of TTF–CA crystal[138] are enlarged by 0.05 Å and 0.012 Å at the NI-transition, a large portion of the transition entropy might arise from the elastic or lattice vibrational origin.

7. Thermochromic Phase Transitions

A variety of transition metal complexes and organometallic compounds change color in the solid state depending on temperature.[139,140] This color change may occur either continuously over a wide temperature range or discontinuously in a narrow temperature interval. The so-called thermochromism known as the reversible dependence of color on temperature has been defined operationally as "an easily noticeable reversible color change occurring in a narrow temperature range, usually accompanied by a phase transition". Regardless of the mechanism responsible for thermochromism this phenomenon involves a change in electronic state of a molecule.

The electronic energy of transition-metal complexes may be perturbed by changes in (i) electron configuration, (ii) coordination geometry, (iii) coordination number, (iv) molecular motion of ligands, and so on. A typical example due to cause (i) is encountered in the spin-crossover complexes described in chapter 3. Thermochromism due to (ii) is observed in structural isomers of coordination compounds. Some nickel complexes are known to exhibit two structural isomers: one is a diamagnetic green form with square-planar coordination geometry and the other is a tetrahedral paramagnetic brown form. In order to elucidate the thermodynamic relationship between these structural isomers, we made calorimetric measurements for bis[*N*-(3-methoxysalicylidene)isopropylaminato]nickel(II)[141] and bis(*N*-isopropyl-5,6-benzosalicylideneiminato)nickel(II).[142] Thermochromism due to (iii) and (iv) will be described in the following sections.

7.1 Thermochromism due to a Change in Coordination Number. A number of copper(II) and nickel(II) halide complexes are known to show thermochromism. Isopropylammonium salts, (*iso*-$PrNH_3$)[$CuCl_3$] and (*iso*-$PrNH_3$)$_2$[$CuCl_4$], exhibit a reversible thermochromic phase transition in the solid state. In the case of (*iso*-$PrNH_3$)[$CuCl_3$], the color of the solid abruptly changes from brown to orange when the crystal is heated above room temperature. Based on X-ray diffraction, NMR, EPR, DSC, and magnetic susceptibility measurements, Roberts et al.[143] revealed that the low-temperature (LT) phase of (*iso*-$PrNH_3$)[$CuCl_3$] belongs to a triclinic crystal system while the high-temperature (HT) phase is orthorhombic, and that the coordination geometry around the central copper atom changes grossly through the thermochromic transition at 324 K: the coordination number of a copper atom changes from five in the LT-phase to six in the HT-phase. The isopropylammonium cations are ordered and hydrogen-bonded to one of the terminal chloride ions in the LT-phase. In contrast, in the HT-phase the isopropylammonium cations are disordered and thereby the hydrogen bonds are weakened. As the result, the terminal chloride ion that is otherwise hydrogen-bonded to isopropylammonium cation bridges two adjacent copper ions. The HT-phase contains tribridged linear chains of $[(CuCl_3)^-]_\infty$, while the LT-phase contains bibridged linear chains of $[(Cu_2Cl_6)^{2-}]_\infty$ (see Fig. 47).

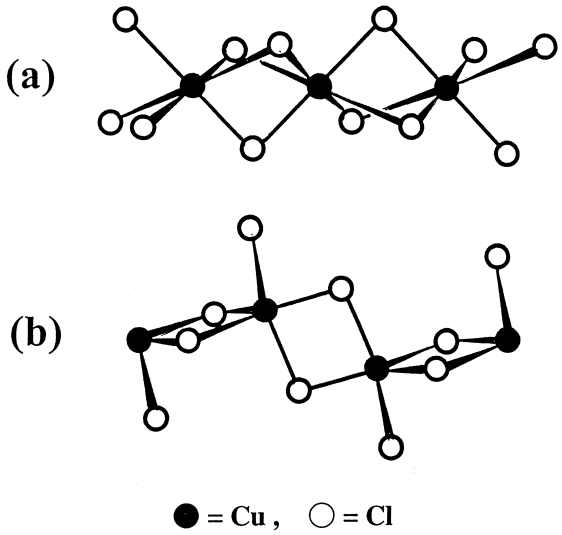

Fig. 47. Coordination geometry of chloride ions (open circles) around the central copper ions (solid circles) schematically drawn according to the X-ray diffraction study by Roberts et al.: (a) The high-temperature phase containing tribridged linear chain of $[(CuCl_3)^-]_n$ and (b) the low-temperature phase containing bibridged linear chain of $[(Cu_2Cl_6)^{2-}]_n$ (Ref. 143).

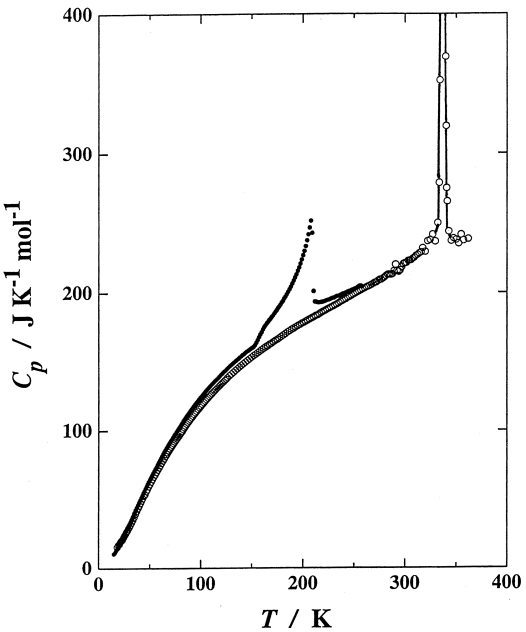

Fig. 48. Molar heat capacity of (*iso*-$PrNH_3$)[$CuCl_3$]. Open and solid circles indicate the stable and the metastable phases, respectively (Ref. 144).

In order to throw more light on this interesting thermochromic phenomenon, we measured its heat capacity by adiabatic calorimetry. Figure 48 represents the molar heat capacity.[144] A phase transition peak was observed at 335.6 K. The enthalpy and entropy gains at the thermochromic phase transition were $\Delta H = 5.54$ kJ mol^{-1} and $\Delta S = 16.5$ J K^{-1} mol^{-1}, respectively. Since the phase transition involves a change of the coordination geometry from five of a nearly square-pyramidal arrange-

ment in the LT-phase to six of an octahedral arrangement in the HT-phase, one would expect a noticeable heat capacity difference between two phases because of a large change in the frequency distribution of lattice vibrations. Contrary to this anticipation, the heat capacity remains almost identical just below and above the phase transition. This fact coincides with the X-ray structural study by Roberts et al.,[143] where the following conclusion was presented: "Although the coordination change around a copper ion appears at first glance to be drastic, the difference between the anion configurations is structurally quite small, only requiring the release of the hydrogen-bonded chloride ion and the movement of each copper by about 0.25 Å, an amount accounted for by thermal motion at room temperature." In other words, the energy difference between two coordination geometries is much smaller than one imagines.

X-ray diffraction analysis and ^{1}H NMR experiments[143] have revealed the onset of two-fold orientational disordering of isopropylammonium cations at the phase transition, which is the basic cause for the coordination geometry change. The LT-phase contains bibridged linear chains of $Cu_2Cl_6^{2-}$ dimers and the isopropylammonium cation is bound to a terminal chloride ion with a N–H···Cl type hydrogen bond. In the HT-phase, the hydrogen bonding is weakened owing to dynamic disorder of isopropylammonium cations and thereby the terminal chloride ion changes its bonding partner from isopropylammonium to two adjacent copper atoms. As a result, the HT-phase contains tribridged linear chains of $(CuCl_3)_\infty^{\infty-}$. Interestingly, the coordination number about each copper atom is larger in the HT-phase than in the LT-phase. It is noted that the volume change is nearly zero for the transition and thus the increased volume due to the dynamic nature of the disorder is just equal to the shrinkage in volume of the copper chloride chain. By taking these situations into account, we can interpret the transition entropy as follows. Of the observed entropy gain, $\Delta S = 16.5$ J K^{-1} mol^{-1}, the two-fold disordering of isopropylammonium cations contributes $R \ln 2$ (= 5.8 J K^{-1} mol^{-1}) to the entropy, while there is substantially no contribution from the acoustic lattice vibrations because of no volume change at the transition. The remaining entropy, 10.7 J K^{-1} mol^{-1}, may be attributed to the excess contribution from the optical metal-ligand skeletal vibrations due to the change in the coordination number.

The HT-phase was easily undercooled and transformed to a metastable LT-phase. The specimen rapidly cooled brought about a higher-order phase transition (solid circles in Fig. 48) without color change at 207.8 K, with enthalpy and entropy changes of $\Delta H = 1.33$ kJ mol^{-1} and $\Delta S = 6.9$ J K^{-1} mol^{-1}. Since no color change was observed at this higher order phase transition, the mechanism responsible for the transition is not a coordination geometry change leading to the thermochromism. The most plausible candidate is the reorientational order-disorder mechanism involving isopropylammonium cations. In fact, the entropy gain is favorably compared with $R \ln 2$ (= 5.8 J K^{-1} mol^{-1}) expected for two-fold orientational disorder of the cation in the HT-phase. The slightly larger contribution of the observed entropy may arise from a change in the lattice vibrations.

As can be seen in Fig. 48, this phase transition is characterized by a stepped heat capacity anomaly appearing around 155 K, which involves enthalpy relaxation characteristic of a glass transition phenomenon. The frozen-in molecular mode below the glass transition temperature might be the reorientational mode of isopropylammonium cation.

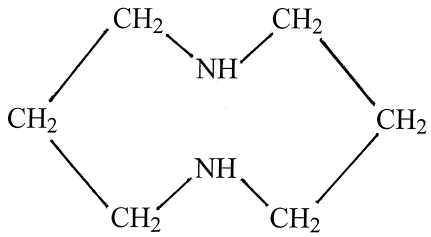

Fig. 49. Molecular structure of eight-membered ring molecule 1,5-diazacyclooctane (daco for short).

7.2 Thermochromism due to Molecular Motion of Ligands. Thermochromism in the square-planar copper(II) complex $[Cu(daco)_2](NO_3)_2$ (daco: 1,5-diazacyclooctane, an eight-membered ring molecule shown in Fig. 49) was found by Yamaki et al.[145] The color of the polycrystal of this complex is brilliant orange as isolated, but it changes to violet discontinuously when heated above 360 K and reverts to orange on cooling. Yamaki et al. thought that coordination of nitrate ions to a copper center at elevated temperatures was responsible for the color change. However, X-ray study of a single crystal by Hoshino et al.[146] revealed that the nitrate ion in the LT-form is far from accessible to the copper atom in the axial direction and instead interacts laterally with the daco-ligands via a pair of hydrogen bonds. Although they did not make an X-ray structural analysis of its HT-form, they claimed that the daco-ligands were bulky enough to preclude coordination of the anions to the copper center even in the HT-phase. Consequently, their conclusion is that the thermochromic mechanism for $[Cu(daco)_2](NO_3)_2$ might involve a ligand-anion interaction rather than metal-anion bonding. However, even if this mechanism is correct, a question is still raised: How is the hydrogen-bonding scheme correlated with the color change and thus the change in the electronic state?

Figure 50 illustrates the molar heat capacity of $[Cu(daco)_2](NO_3)_2$ determined by adiabatic calorimetry.[147] A large heat capacity anomaly associated with the thermochromic phenomenon was found at 359 K. This phase transition exhibits both superheating and undercooling effects, indicating a first-order phase transition. The thermodynamic quantities due to the phase transition were $\Delta H = (8.40 \pm 0.22)$ kJ mol^{-1} and $\Delta S = (23.4 \pm 0.8)$ J K^{-1} mol^{-1}. From a thermodynamic viewpoint, the entropy gain at a phase transition plays a diagnostic role in the elucidation of the transition mechanism. The large entropy gain observed here implies that softening of molecular or lattice vibrations and/or onset of orientational disordering of the daco ligand or the nitrate anion would be involved in the phase transition. For the present thermochromic compound, however, the possibility of softening of optical vibrational modes is precluded, because the IR spectra showed no detectable shift of absorption bands on going from one phase to the other.[147] We speculated that dynamic interconversion of a daco-ligand between a chair and a boat form might take place in the HT-phase. If this is the case, each daco-ring will gain

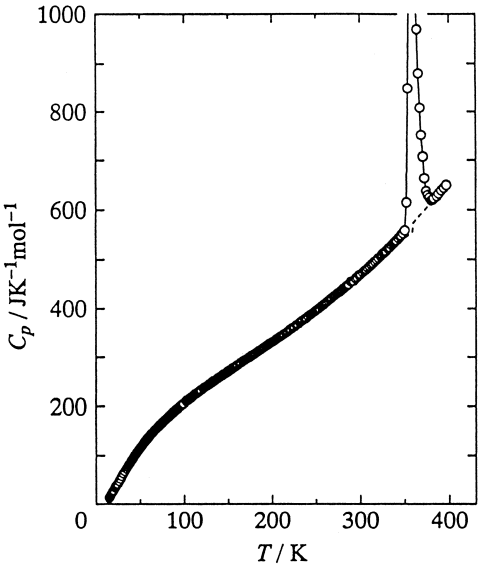

Fig. 50. Molar heat capacity of the thermochromic compound $[Cu(daco)_2](NO_3)_2$. Broken curve shows the normal heat capacity and solid lines are guide for eye (Ref. 147).

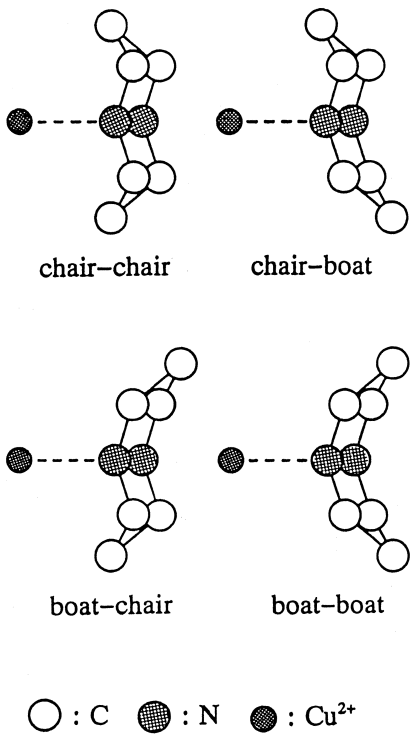

Fig. 51. Schematic drawing of four conformations of the eight-membered daco ring having almost equal energy (Ref. 147).

four conformations as shown in Fig. 51 (i.e. chair–chair, chair–boat, boat–chair, and boat–boat), and the total number of conformations per $[Cu(daco)_2]^{2+}$ cation amounts to 16 ($= 4 \times 4$), because a cation contains two daco-ligands. According to the Boltzmann principle, the conformational entropy is estimated to be R ln 16 ($= 23.05$ J K^{-1} mol^{-1}). This entropy gain accounts surprisingly well for the observed transition entropy of $\Delta S = (23.4 \pm 0.8)$ J K^{-1} mol^{-1}.

We shall discuss the relationship between the color change and the change in the electronic state of the $[Cu(daco)_2]^{2+}$ ion. A single crystal X-ray study by Hoshino et al.[146] revealed that the structure is centrosymmetric with the center of symmetry on the site of Cu, and the CuN_4 chelate plane is planar, but it is not precisely square since the two Cu–N coordination bonds of a daco-ligand differ in length significantly. On the other hand, in the HT-phase eight-membered daco-ligands undergo dynamic conformational changes between the boat and chair forms, and thereby the CuN_4 chelate plane is dynamically distorted from a planar form probably to a distorted tetrahedral coordination geometry. When such a planar-to-tetrahedral geometrical change occurs, a red shift in the *d–d* transition is expected, as indicated by a theoretical angular overlap method.[148] The visible spectrum of $[Cu(daco)_2](NO_3)_2$ indeed exhibits such a red shift.[145,146]

A quite similar situation has been encountered in a homologous series of thermochromic complexes with formula $[M(dieten)_2]X_2$, where M is Cu(II) or Ni(II), dieten is *N*,*N*-diethylethylenediamine, and X is BF_4^- or ClO_4^-. The copper complexes show a color change from red to blue-violet and color of the nickel complexes changes from orange to red when they undergo phase transition in the solid state. It was initially thought that the thermochromism was caused by axial approach of the anions to the copper or nickel ion. However, when the crystal structures of both the LT- and HT-phases were determined, that idea turned out to be wrong.[149,150] There exists no axial coordination of the counter anions in either of the phases because the bulky alkyl groups bonded to the nitrogen atoms prevent the counter anions from approaching the central metal atom. A new mechanism of thermochromism was proposed as follows: in the HT-phase the chelate rings pucker up and down while they remain static in the LT-phase. Such ring motion affects the ligand field strength, leading to the color change. This mechanism seems to be consistent with various experimental results so far available. However, the relationship between the microscopic aspects[149–153] hitherto reported and the macroscopic energetic and entropic aspects was still unclear.

In order to gain more quantitative insight into the thermochromic mechanism of the series of complexes, we measured their heat capacities by adiabatic calorimetry.[154–156] Figure 52 represents the molar heat capacity of $[Cu(dieten)_2](ClO_4)_2$.[155] A large single peak due to the thermochromic phase transition was found at 317.64 K. This phase transition is characterized by a long heat-capacity tail extending down to about 200 K. Moreover, the normal heat capacity curve has a jump of 46 J K^{-1} mol^{-1} at the transition temperature between the LT- and HT-phases. Thermodynamic gains were $\Delta H = 17.4$ kJ mol^{-1} and $\Delta S = 55.2$ J K^{-1} mol^{-1}. As summarized in Table 8, the other three complexes also exhibited similar phase transitions.[154,156]

X-ray diffraction analysis[149,150] provides a useful clue to the molecular freedom responsible for the entropy gain. The most remarkable change in the structure occurring through the phase transition is the motion of the chelate rings, which is easily seen from anisotropic thermal ellipsoids of the constituent atoms. The chelate rings are puckering up and down from the

Table 8. Comparison of the Observed and Theoretical Quantities for the Thermochromic Phase Transitions in $[Cu(dieten)_2]X_2$ (X = BF_4^- and ClO_4^-). T_{trs}, ΔH(obsd), and ΔS(obsd) Are Observed Transition Temperature, Enthalpy and Entropy of Transition, Respectively. ΔH(ligand) and ΔC(ligand) Are Calculated for a Model of Chelate Ring Puckering Motion. ΔC_p(obsd) Indicates the Gap of the Normal Heat Capacity at T_{trs}. ΔH(AOM) Is the Enthalpy Gain due to the Change in the *d*-Electronic State. ΔH(total) Is the Sum of ΔH(ligand) and ΔH(AOM)

Complex	T_{trs}	ΔH(obsd)	ΔS(obsd)	ΔC_p(obsd)	ΔC(ligand)	ΔH(ligand)	ΔH(AOM)	ΔH(total)
	K	kJ mol^{-1}	J K^{-1} mol^{-1}	J K^{-1} mol^{-1}	J K^{-1} mol^{-1}	kJ mol^{-1}	kJ mol^{-1}	kJ mol^{-1}
$[Cu(dieten)_2](BF_4)_2$	302.64	16.6	55.3	16	33	7.7	9.1	16.8
$[Cu(dieten)_2](ClO_4)_2$	317.64	17.4	55.2	46	33	8.0	8.4	16.4
$[Ni(dieten)_2](BF_4)_2$	374.86	20.9	57.4	12			15.7	
$[Ni(dieten)_2](ClO_4)_2$	382.01	20.2	54.7	48			12.0	

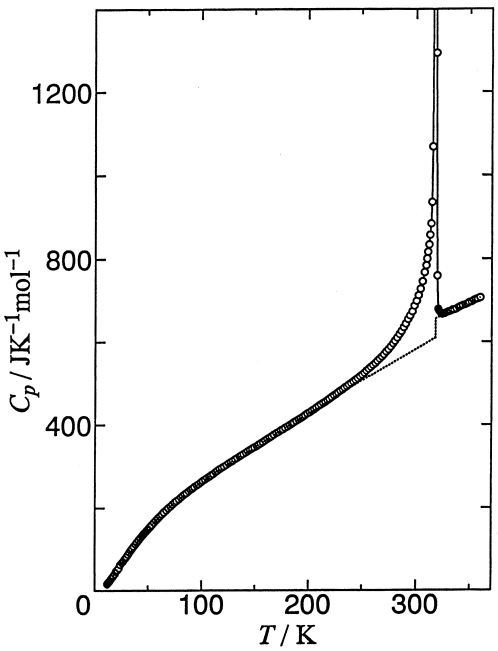

Fig. 52. Molar heat capacity of the thermochromic compound $[Cu(dieten)_2](ClO_4)_2$. Dotted curves shows the normal heat capacities of the LT- and HT-phases, resulting a heat-capacity jump at the transition temperature. The solid lines are only guides for the eye (Ref. 155).

CuN_4 plane in the HT-phase. Provided that this chelate ring puckering is responsible for an essential part of the transition mechanism, we can estimate the enthalpy gain at the phase transition as follows. Let us assume that the chelate rings are static at very low temperatures, whereas they pucker in the HT-phase. There are two chelate rings in a cation, consisting of a five-membered CuN_2C_2 ring. When the plane formed by the CuN_2 is fixed, the five-membered ring has four different configurations: two configurations in which two carbon atoms are tipped off to the same side of the plane and two configurations in which two carbon atoms are tipped off to the opposite sides of the plane. It should be remarked that the number of degrees of freedom for the puckering motion of a five-membered ring is two. Moreover, since there exist two chelate rings in a cation, so the total number of the puckering modes amounts to four. These four modes are roughly assumed to be degenerate and can be simply approximated by the Einstein harmonic oscillator. If we assume that this puckering motion is responsible for the total entropy of transition, the Einstein characteristic frequency is estimated to be 115 cm^{-1} for $[Cu(diet\text{-}en)_2](ClO_4)_2$. Based on this frequency, we estimated the heat-capacity jump at the transition temperature as ΔC(ligand) = 33 J K^{-1} mol^{-1} and ΔH(ligand) = 8.0 kJ mol^{-1}. The heat-capacity jump is comparable with the observed value of 46 J K^{-1} mol^{-1}. The contribution of the chelate-ring puckering ΔH(ligand) to the observed ΔH(obsd) is about 46 per cent.

According to the X-ray structural analysis of $[Cu(dieten)_2](ClO_4)_2$,[149,150] there is no significant change in the Cu–N distances, whereas the *trans* bond angles of N–Cu–N change slightly through the phase transition. In the LT-phase the angles are 180.0°, while in the HT-phase they are 178.0° and 174.7°. The $[Cu(dieten)_2]^{2+}$ cation is characterized by a square-planar coordination geometry in the LT-phase. This geometry is slightly distorted toward a tetrahedral coordination in the HT-phase. Despite such a small geometrical change, the color of complexes changes dramatically when the phase transition occurs. The color of the complexes depends obviously on the absorption of visible light by a molecule. The absorption spectra in the visible region depend on the energy-level splitting of the *d*-orbitals. Variable-temperature *d*–*d* transition of $[M(dieten)_2]X_2$ has already been studied.[151,152] These complexes show a red shift in the *d*–*d* transition when they are heated. To investigate the relationship between the absorption spectra and the *d*-orbital energy levels, the angular overlap model (AOM)[148] was adopted. The relative energies of the five *d*-orbitals can be calculated as a function of the polar angles (θ, ϕ) of the ligand position vectors. The calculated energy levels are illustrated in Fig. 53 as a function of θ.[155] The visible light absorption maximum (ν_{max}) is shifted from 20700 cm^{-1} in the LT-phase to 19305 cm^{-1} in the HT-phase for $[Cu(dieten)_2](ClO_4)_2$.[151,152] The absorption maximum in the electronic spectrum corresponds to the d_{yz}, $d_{xz} \rightarrow d_{x^2-y^2}$ transition. Namely, the transition energy is the energy difference between these two orbitals, $\Delta E(\theta)$ in Fig. 53. In the LT-phase, since the coordination geometry is D_{4h}, $\Delta E(90)$ is equal to the absorption maximum observed at lower temperature, while in the HT-phase $\Delta E(\theta)$ is equal to the absorption maximum recorded at higher temperature. Therefore the following relation is obtained:

$$\frac{\Delta E(90)}{\Delta E(\theta)} = \frac{h\nu_{max} \text{ at low temperature}}{h\nu_{max} \text{ at high temperature}}.$$

The enthalpy (actually the internal energy) of the *d*-orbitals is the sum of each electron's energy. The *d*-electrons are ac-

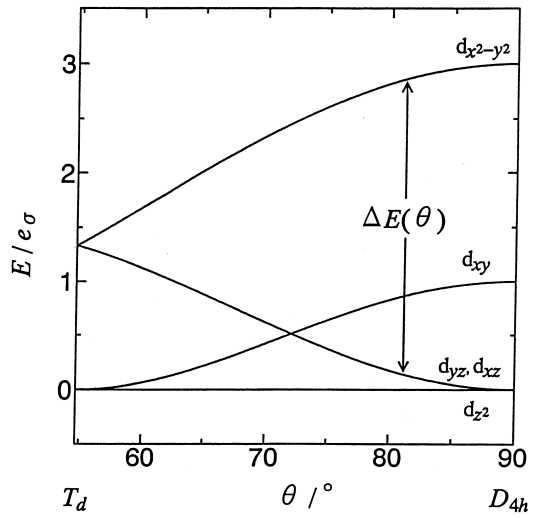

Fig. 53. Energy level diagram correlating tetrahedral and planar coordination geometries calculated on the basis of the angular overlap model (Ref. 155).

commodated in the energy level diagram shown in Fig. 53, one by one from bottom to top. There are nine *d*-electrons in the copper complexes. The energy of the *d*-orbitals in the LT-phase is calculated from the energy scheme at $\theta = 90°$, whereas that in the HT-phase is calculated from the scheme at the θ estimated from the equation given above. Consequently, the enthalpy change of the *d*-orbitals arising from the change in the coordination geometry is straightforwardly determined as the difference between the electron energies of the LT- and the HT-phases. The contribution of the *d*-orbital energy to the transition enthalpy was 8.4 kJ mol^{-1} for [Cu(dieten)$_2$](ClO$_4$)$_2$.

We have so far regarded the observed transition enthalpy as consisting of two contributions: one is the enthalpy gain due to the onset of the puckering motion of the metal-ligand chelate rings and the other is the electronic energy gained by a change in the coordination geometry across the phase transition. These two contributions were analyzed in terms of the harmonic oscillator model and the angular overlap model, respectively. As shown in Table 8, the former is ΔH(ligand) = 8.0 kJ mol^{-1} and the latter amounts to ΔH(AOM) = 8.4 kJ mol^{-1}. The sum of these contributions corresponds to ΔH(total) = 16.4 kJ mol^{-1}. Surprisingly this theoretical value well accounts for the observed value, ΔH(obsd) = 17.4 kJ mol^{-1}. Even better agreement has been attained for [Cu(dieten)$_2$](BF$_4$)$_2$, in which ΔH(obsd) and ΔH(total) are 16.6 and 16.8 kJ mol^{-1}, respectively.

8. Concluding Remarks

Heat capacity is a physical quantity containing contributions from all kinds of molecular degrees of freedom at the rate of the Maxwell–Boltzmann distribution. This makes a sharp contrast with various spectroscopies in which particular nuclide and/or particular modes are selectively sensed. In other words, thermodynamic measurements are not restricted by any selection rules or selectivity. Consequently calorimetries are applicable to a wide range of researches. Modern sciences are greatly specialized in an individual field of study. Therefore, better understanding of materials should be achieved by employing complementarily experimental techniques which lead either to microscopic aspects or to macroscopic aspects.

The studies described here have been achieved in collaboration with many coworkers, colleagues, and students. On this occasion the author would like to express his sincere thanks to Emeritus Prof. Syûzô Seki, Emeritus Prof. Hiroshi Suga, and Emeritus Prof. Sei Otsuka (Osaka University), Prof. Philipp Gütlich and Dr. Jürgen Ensling (University of Mainz), Prof. David N. Hendrickson (University of California at San Diego), Emeritus Prof. Hirotoshi Sano (Tokyo Metropolitan University), Prof. Takeshi Kambara (the University of Electro-Communications), Prof. Yonezo Maeda (Kyushu University), Prof. Norimichi Kojima (the University of Tokyo), Prof. Hiroshi Kitagawa (University of Tsukuba), Prof. Leslie F. Larkworthy (University of Surrey), Mr. Shigemi Murakawa, Mr. Yutaka Shiomi, Mr. Tomio Wakamatsu, Dr. Kazutoshi Kaji, Dr. Motohiro Nakano, Dr. Akihito Nishimori, Dr. Yatsuhisa Nagano, Ms. Yuki Kaneko, Ms. Yohko Yumoto, Ms. Tomoko Kawamura, Ms. Hisako Hara, Dr. Yuji Miyazaki, Dr. Qi Wang, Dr. Ashis Bhattacharjee, and Dr. Tadahiro Nakamoto (Osaka University). This work was partially supported by a Grant-in-Aid for Scientific Research on Priority Areas "Metal-Assembled Complexes" (Area No. 401/12023229) from the Ministry of Education, Science, Sports and Culture.

References

1 N. G. Personage and L. A. K. Staveley, "Disorder in Crystals," Oxford University Press, London (1978).

2 R. L. Carlin, "Magnetochemistry," Springer-Verlag, Berlin (1986).

3 M. Sorai, "Heat-Capacity Calorimetry of Molecule-Based Magnetic Materials," in "Molecule-Based Magnetic Materials: Theory, Techniques, and Application," ed by M. M. Turnbull, T. Sugimoto, and L. K. Thompson, ACS Symposium Series 644, American Chemical Society (1996), Chapter 7, pp. 99–114.

4 M. Sorai, Y. Miyazaki, and T. Hashiguchi, "Heat Capacity Studies of Organic Radical Crystals," in "Magnetic Properties of Organic Materials," ed by P. M. Lahti, Marcel Dekker, Inc., New York (1999), Chap.23, pp. 475–490.

5 M. Sorai, H. Suga, and S. Seki, *Bull. Chem. Soc. Jpn.*, **41**, 312 (1968).

6 N. Arai, M. Sorai, H. Suga, and S. Seki, *Bull. Chem. Soc. Jpn.*, **50**, 1702 (1977).

7 S. Murakawa, T. Wakamatsu, M. Nakano, M. Sorai, and H. Suga, *J. Chem. Thermodyn.*, **19**, 1275 (1987).

8 M. Sorai, A. Nishimori, and Y. Nagano, unpublished results.

9 M. Sorai, K. Kaji, and Y. Kaneko, *J. Chem. Thermodyn.*, **24**, 167 (1992).

10 K. Saito, Y. Yamamura and M. Sorai, *Netsu Sokutei (Calorimetry and Thermal Analysis)*, **26**, 150 (1998).

11 M. Sorai, A. Kosaki, H. Suga, S. Seki, T. Yoshida, and S. Otsuka, *Bull. Chem. Soc. Jpn.*, **44**, 2364 (1971).

12 S. Otsuka, A. Nakamura, and T. Yoshida, *Inorg. Chem.*, **7**, 261 (1968).

13 S. Otsuka, A. Nakamura, and T. Yoshida, *Liebigs Ann. Chem.*, **719**, 54 (1968).

14 P. D. Frisch and L. F. Dahl, *J. Am. Chem. Soc.*, **94**, 5082

(1972).
15 N. Kamijo and T. Watanabe, *Acta Crystallogr., Sect. B*., **35**, 2537 (1979).
16 J. W. Edwards, G. L. Kington, and R. Mason, *Trans. Faraday Soc*., **56**, 660 (1960).
17 C. R. Pulliam, J. B. Thoden, A. M. Stacy, B. Spencer, M. H. Englert, and L. F. Dahl, *J. Am. Chem. Soc*., **113**, 7398 (1991).
18 P. D. Frisch and L. F. Dahl, *J. Am. Chem. Soc*., **94**, 5082 (1972).
19 D. B. Chesnut, *J. Chem. Phys*., **40**, 405 (1964).
20 Y. Tanabe and S. Sugano, *J. Phys. Soc. Jpn*., **9**, 753, 766 (1954).
21 E. König and K. Madeja, *Inorg. Chem*., **6**, 48 (1967).
22 W. A. Baker, J. And H. M. Bobonich, *Inorg. Chem*., **3**, 1184 (1964).
23 M. Sorai and S. Seki, *J. Phys. Soc. Jpn*., **33**, 575 (1972).
24 M. Sorai and S. Seki, *J. Phys. Chem. Solids*, **35**, 555 (1974).
25 J. H. Takemoto and B. Hutchinson, *Inorg. Chem*., **12**, 705 (1973).
26 P. Gütlich, A. Hauser, and H. Spiering, *Angew. Chem., Int. Ed. Engl*., **33**, 2024 (1994).
27 G. A. Renovitch and W. A. Baker, Jr., *J. Am. Chem. Soc*., **89**, 6377 (1967).
28 M. Sorai, J. Ensling, K. M. Hasselbach, and P. Gütlich, *Chem. Phys*., **20**, 197 (1977).
29 A. M. Greenaway and E. Sinn, *J. Am. Chem. Soc*., **100**, 8080 (1978).
30 M. Mikami, M. Konno, and Y. Saito, *Chem. Phys. Lett*., **63**, 566 (1979).
31 B. Katz and C. E. Strouse, *J. Am. Chem. Soc*., **101**, 6214 (1979).
32 A. M. Greenaway, C. J. O'Connor, A. Schrock, and E. Sinn, *Inorg. Chem*., **18**, 2692 (1979).
33 M. Mikami, M. Konno, and Y. Saito, *Acta Crystallogr. Sect. B*, **36**, 275 (1980).
34 B. Katz and C. E. Strouse, *Inorg. Chem*., **19**, 658 (1980).
35 M. Mikami-Kido and Y. Saito, *Acta Crystallogr., Sect. B*., **38**, 452 (1982).
36 L. Wiehl, G. Kiel, C. P. Köhler, H. Spiering, and P. Gütlich, *Inorg. Chem*., **25**, 1565 (1986).
37 K. Kaji and M. Sorai, *Thermochim. Acta*, **88**, 185 (1985).
38 H. Köppen, E. W. Müller, C. P. Köhler, H. Spiering, E. Meissner, and P. Gütlich, *Chem. Phys. Lett*., **91**, 348 (1982).
39 N. Sasaki and T. Kambara, *Phys. Rev. B, Condens. Matter*, **40**, 2442 (1989).
40 J.-A. Real, H. Bolvin, A. Bousseksou, A. Dwarkin, O. Kahn, F. Varret, and J. Zarembowitch, *J. Am. Chem. Soc*., **114**, 4650 (1992).
41 H. Romstedt, A. Hauser, and H. Spiering, *J. Phys. Chem. Solids*, **59**, 265 (1998).
42 H. Romstedt, H. Spiering, and P. Gütlich, *J. Phys. Chem. Solids*, **59**, 1353 (1998).
43 Y. Garcia, O. Kahn, L. Rabardel, B. Chansou, L. Salmon, and J.-P. Tuchagues, *Inorg. Chem*., **38**, 4663 (1999).
44 M. Sorai and S. Seki, *J. Phys. Soc. Jpn*., **32**, 382 (1972).
45 T. Nakomoto, Z.-C. Tan, and M. Sorai, *Inorg. Chem*., **40**, 3805 (2001).
46 T. Nakamoto, A. Bhattacharjee, and M. Sorai, the 50th Annual Meeting on Coordination Chemistry, Kusatsu, 1H-F10 (2000).
47 M. Sorai, J. Ensling, and P. Gütlich, *Chem. Phys*., **18**, 199 (1976).
48 P. Gütlich, R. Link, and H. G. Steinhäuser, *Inorg. Chem*., **17**, 2509 (1978).
49 K. Kaji, and M. Sorai, the 36th Annual Meeting on Coordination Chemistry, Nagoya, 2B08 (1986).
50 R. Jakobi, H. Spiering, L. Wiehl, E. Gmelin, and P. Gütlich, *Inorg. Chem*., **27**, 1823 (1988).
51 R. Jakobi, H. Spiering, and P. Gütlich, *J. Phys. Chem. Solids*, **53**, 267 (1992).
52 R. Jakobi, H. Romstedt, H. Spiering, and P. Gütlich, *Angew. Chem., Int. Ed. Engl*., **31**, 178 (1992).
53 M. S. Haddad, W. D. Federer, M. W. Lynch, and D. N. Hendrickson, *J. Am. Chem. Soc*., **102**, 1468 (1980).
54 M. S. Haddad, M. W. Lynch, W. D. Federer, and D. N. Hendrickson, *Inorg. Chem*., **20**, 123 (1981).
55 M. S. Haddad, W. D. Federer, M. W. Lynch, and D. N. Hendrickson, *Inorg. Chem*., **20**, 131 (1981).
56 M. Sorai and D. N. Hendrickson, The 37th Annual Meeting on Coordination Chemistry, Tokyo, 2B14 (1987).
57 H. G. Drickamer and C. W. Frank, "Electronic Transitions and the High Pressure Chemistry and Physics of Solids," Chapman and Hall, London (1973).
58 D. M. Halepoto, D. G. L. Holt, L. F. Larkworthy, G. J. Leigh, D. C. Povey, and G. W. Smith, *J. Chem. Soc., Chem. Commun*., **1989**, 1322.
59 M. Sorai, Y. Yumoto, D. M. Halepoto and L. F. Larkworthy, *J. Phys. Chem. Solids*, **54**, 421 (1993).
60 M. Sorai, Y. Maeda, and H. Oshio, *J. Phys. Chem. Solids*, **51**, 941 (1990).
61 J. Frenkel, "Kinetic Theory of Liquids," Oxford University Press, London (1947).
62 P. E. Doan and B. R. McGarvey, *Inorg. Chem*., **29**, 874 (1990).
63 A. J. Conti, R. K. Chadha, K. M. Sena, A. L. Rheingold, and D. N. Hendrickson, *Inorg. Chem*., **32**, 2670 (1993).
64 A. J. Conti, K. Kaji, Y. Nagano, K. M. Sena, Y. Yumoto, R. K. Chadha, A. L. Rheingold, M. Sorai, and D. N. Hendrickson, *Inorg. Chem*., **32**, 2681 (1993).
65 K. Kaji, M. Sorai, A. J. Conti, and D. N. Hendrickson, *J. Phys. Chem. Solids*, **54**, 1621 (1993).
66 M. Sorai, Y. Nagano, A. J. Conti and D. N. Hendrickson, *J. Phys. Chem Solids*, **55**, 317 (1994).
67 M. Sorai, Y. Yumoto, and D. N. Hendrickson, the 42nd Annual Meeting on Coordination Chemistry, Nara, 3B08 (1992).
68 "Mixed-Valence Compounds, Theory and Applications in Chemistry, Physics, Geology, and Biology," ed by D. B. Brown, Reidel, Boston (1980).
69 P. Day, *Int. Rev. Phys. Chem*., **1**, 142 (1981).
70 C. Creutz, *Prog. Inorg. Chem*., **30**, 1 (1983).
71 D. E. Richardson and H. Taube, *Coord. Chem. Rev*., **60**, 107 (1984).
72 "Mixed Valency Systems: Applications in Chemistry, Physics and Biology," ed by K. Prassides, Kluwer, Boston (1991).
73 S. E. Woehler, R. J. Wittebort, S. M. Oh, T. Kambara, D. N. Hendrickson, D. Inniss, and C. E. Strouse, *J. Am. Chem. Soc*., **109**, 1063 (1987).
74 S. M. Oh, D. N. Hendrickson, K. L. Hassett, and R. E. Davis, *J. Am. Chem. Soc*., **106**, 7984 (1984).
75 S. M. Oh, D. N. Hendrickson, K. L. Hassett, and R. E. Davis, *J. Am. Chem. Soc*., **107**, 8009 (1985).
76 M. Sorai and D. N. Hendrickson, *Pure & Appl. Chem*., **63**, 1503 (1991).

77 D. N. Hendrickson, in "Mixed Valency Systems: Applications in Chemistry, Physics and Biology," ed by K. Prassides, Kluwer, Boston, 67 (1991).
78 J. P. Launay and F. Babonneau, *Chem. Phys.*, **67**, 295 (1982).
79 S. A. Borshch, I. N. Kotov, and I. B. Bersuker, *Chem. Phys. Lett.*, **89**, 381 (1982).
80 R. D. Cannon, L. Montri, D. B. Brown, K. M. Marshall, and C. M. Elliot, *J. Am. Chem. Soc.*, **106**, 2591 (1984).
81 T. Kambara, D. N. Hendrickson, M. Sorai, and S. M. Oh, *J. Chem. Phys.*, **85**, 2895 (1986).
82 M. Nakano, M. Sorai, J. B. Vincent, G. Christou, Ho G. Jang, and D. N. Hendrickson, *Inorg. Chem.*, **28**, 4608 (1989).
83 S. M. Oh, T. Kambara, D. N. Hendrickson, M. Sorai, K. Kaji, S. E. Woehler, and R. J. Wittebort, *J. Am. Chem. Soc.*, **107**, 5540 (1985).
84 M. Sorai, K. Kaji, D. N. Hendrickson, and S. M. Oh, *J. Am. Chem. Soc.*, **108**, 702 (1986).
85 Ho G. Jang, J. B. Vincent, M. Nakano, J. C. Huffman, G. Christou, M. Sorai, R. J. Wittebort, and D. N. Hendrickson, *J. Am. Chem. Soc.*, **111**, 7778 (1989).
86 Ho G. Jang, S. J. Geib, Y. Kaneko, M. Nakano, M. Sorai, A. L. Rheingold, B. Montez, and D. N. Hendrickson, *J. Am. Chem. Soc.*, **111**, 173 (1989).
87 Y. Kaneko, M. Nakano, M. Sorai, Ho G. Jang, and D. N. Hendrickson, *Inorg. Chem.*, **28**, 1067 (1989).
88 Ho G. Jang, R. J. Wittebort, M. Sorai, Y. Kaneko, M. Nakano and D. N. Hendrickson, *Inorg. Chem.*, **31**, 2265 (1992).
89 M. Sorai, Y. Shiomi, D. N. Hendrickson, S. M. Oh, and T. Kambara, *Inorg. Chem.*, **26**, 223 (1987).
90 A. Nishimori, Y. Nagano, M. Sorai, and D. N. Hendrickson, the 22nd Annual Meeting of the Japan Society of Calorimetry and Thermal Analysis, Tsukuba, D310 (1986).
91 Ho G. Jang, K. Kaji, M. Sorai, R. J. Wittebort, S. J. Geib, A. L. Rheingold, and D. N. Hendrickson, *Inorg. Chem.*, **29**, 3547 (1990).
92 T. Nakamoto, M. Hanaya, M. Katada, K. Endo, S. Kitagawa, and H. Sano, *Inorg. Chem.*, **36**, 4347 (1997).
93 R. M. Stratt and S. H. Adachi, *J. Chem. Phys.*, **86**, 7156 (1987).
94 T. Nakamoto, M. Katada, and H. Sano, *Chem. Lett.*, **1990**, 225.
95 T. Nakamoto, M. Katada, and H. Sano, *Inorg. Chim. Acta*, **291**, 127 (1999).
96 M. Sorai, T. Nakamoto, M. Katada, S. Kitagawa, H. Sano, and K. Endo, the 45th Japanese Annual Meeting on Coordination Chemistry, Fukuoka, 1B05 (1995).
97 M. Sorai, A. Bhattacharjee, T. Nakamoto, M. Katada, S. Kitagawa, H. Sano, and K. Endo, the 49th Japanese Annual Meeting on Coordination Chemistry, Sapporo, 3G3-F07 (1999).
98 S. B. Piepho, E. R. Krausz, and P. N. Schatz, *J. Am. Chem. Soc.*, **100**, 2996 (1978).
99 D. N. Hendrickson, S. M. Oh, T.-Y. Dong, T. Kambara, M. J. Cohn, and M. F. Moore, *Comments Inorg. Chem.*, **4**, 329 (1985).
100 T. Kambara, D. N. Hendrickson, T.-Y. Dong, and M. J. Cohn, *J. Chem. Phys.*, **86**, 2362 (1987).
101 S. I. Klokishner and B. S. Tsukerblat, *Chem. Phys.*, **125**, 11 (1988).
102 A. V. Koryachenko, S. I. Klokishner and B. S. Tsukerblat, *Chem. Phys.*, **150**, 295 (1991).
103 M. J. Cohn, T.-Y. Dong, D. N. Hendrickson, S. J. Geib, and A. L. Rheingold, *J. Chem. Soc., Chem. Commun.*, **1985**, 1095.
104 S. Iijima, R. Saida, I. Motoyama, and H. Sano, *Bull. Chem. Soc. Jpn.*, **54**, 1375 (1981).
105 T.-Y. Dong, D. N. Hendrickson, K. Iwai, M. J. Cohn, A. L. Rheingold, H. Sano, I. Motoyama, and S. Nakashima, *J. Am. Chem. Soc.*, **107**, 7996 (1985).
106 R. J. Webb, P. M. Hagen, R. J. Wittebort, M. Sorai, and D. N. Hendrickson, *Inorg. Chem.*, **31**, 1791 (1992).
107 M. Sorai, A. Nishimori, D. N. Hendrickson, T. Y. Dong, and M. J. Cohn, *J. Am. Chem. Soc.*, **109**, 4266 (1987).
108 S. Nakashima, A. Nishimori, Y. Masuda, H. Sano, and M. Sorai, *J. Phys. Chem. Solids*, **52**, 1169 (1991).
109 W. H. Morrison, Jr. And D. N. Hendrickson, *Inorg. Chem.*, **14**, 2331 (1975).
110 I. Motoyama, K. Suto, M. Katada, and H. Sano, *Chem. Lett.*, **1983**, 1215.
111 T.-Y. Dong, D. N. Hendrickson, C. G. Piepont, and M. F. Moor, *J. Am. Chem. Soc.*, **108**, 963 (1986).
112 M. Nakano, M. Sorai, P. M. Hagen and D. N. Hendrickson, *Chem. Phys. Lett.*, **196**, 486 (1992).
113 T. Kambara and N. Sasaki, *J. Coord. Chem.*, **18**, 129 (1988).
114 H. Kitagawa, N. Onodera, J.-S. Ahn, T. Mitani, M. Kim, Y. Ozawa, K. Toriumi, K. Yasui, T. Manabe, and M. Yamashita, *Mol. Cryst. Liq. Cryst.*, **285**, 311 (1996).
115 H. Kitagawa, N. Onodera, J.-S. Ahn, T. Mitani, K. Toriumi, and M. Yamashita, *Synth. Met.*, **86**, 1931 (1997).
116 H. Kitagawa, N. Onodera, T. Sonoyama, M. Yamamoto, T. Fukawa, T. Mitani, M. Seto, and Y. Maeda, *J. Am. Chem. Soc.*, **121**, 10068 (1999).
117 H. Kitagawa and T. Mitani, *Coord. Chem. Rev.*, **190-192**, 1169 (1999).
118 M. Kim, K. Tanaka, Y. Ozawa, and K. Toriumi, manuscript in preparation.
119 Y. Miyazaki, Q. Wang, A. Sato, K. Saito, M. Yamamoto, H. Kitagawa, T. Mitani, and M. Sorai, *J. Phys. Chem. B*, (2001). In press.
120 N. Kojima, W. Aoki, M. Seto, Y. Kobayashi, and Yu. Maeda, *Synthetic Metals*, **121**, 1796 (2001).
121 N. Kojima, W. Aoki, M. Itoi, Y. Ono, M. Seto, Y. Kobayashi, and Yu. Maeda, Solid State Commun., **120**, 165 (2001).
122 H. Tamaki, Z. J. Zhong, N. Matsumoto, S. Kida, M. Koikawa, N. Achiwa, Y. Hashimoto, and H. Okawa, *J. Am. Chem. Soc.*, **114**, 6974 (1992).
123 S. Decurtins, H. W. Schmalle, H. R. Oswald, A. Linden, J. Ensling, P. Gütlich, and A. Hauser, *Inorg. Chim. Acta*, **216**, 65 (1994).
124 T. Nakamoto, Y. Miyazaki, M. Itoi, Y. Ono, N. Kojima, and M. Sorai, *Angew. Chem., Int. Ed.*, (2001). In press.
125 A. Bhattacharjee, Y. Miyazaki, and M. Sorai, *J. Phys. Soc. Jpn.*, **69**, 479 (2000).
126 J. B. Torrance, A. Girlando, J. J. Mayerle, J. I. Crowley, V. Y. Lee, P. Batail, and S. J. LaPlaca, *Phys. Rev. Lett.*, **47**, 1747 (1981).
127 Y. Iwasa, T. Koda, Y. Tokura, A. Kobayashi, N. Iwasawa, and G. Saito, *Phys. Rev. B*, **42**, 2374 (1990).
128 S. Aoki, T. Nakayama, and A. Miura, *Phys. Rev. B*, **48**, 626 (1993).
129 S. Aoki and T. Nakayama, *Phys. Rev. B*, **56**, R2893 (1997).
130 C. S. Jacobsen and J. B. Torrance, *J. Chem. Phys.*, **78**, 112 (1983).
131 A. Girlando, F. Marzola, C. Pecile, J. B. Torrance, *J. Chem.*

Phys., **79**, 1075 (1983).
132 T. Mitani, G. Saito, Y. Tokura, and T. Koda, *Phys. Rev. Lett*., **53**, 842 (1984).
133 K. Takaoka, Y. Kaneko, H. Okamoto, Y. Tokura, T. Koda, T. Mitani, and G. Saito, *Phys. Rev. B*, **36**, 3884 (1987).
134 K. Kikuchi, K. Yakushi, and H. Kuroda, *Solid State Commun*., **44**, 151 (1982).
135 T. Kawamura, Y. Miyazaki and M. Sorai, *Chem. Phys. Lett*., **273**, 435 (1997).
136 Y. Miyazaki, Y. Iida, and M. Sorai, the 35th Annual Meeting of Calorimetry and Thermal Analysis, Tokyo, 2C0940 (1999).
137 J. J. Mayerle, J. B. Torrance, and J. I. Crowley, *Acta Crystallogr.*, **B35**, 2988 (1979).
138 M. Le Cointe, M. H. Lemée-Cailleau, H. Cailleau, B. Toudic, L. Toupet, G. Heger, F. Moussa, P. Schweiss, K. H. Kraft, and N. Karl, *Phys. Rev. B*, **51**, 3374 (1995).
139 D. R. Bloomquist and R. D. Willett, *Coord. Chem. Rev.*, **47**, 125 (1982).
140 K. Sone and Y. Fukuda, "Inorganic Thermochromism, (Inorganic Chemistry Concepts, Vol. 10)," Springer Verlag, Berlin (1987).
141 N. Arai, M. Sorai, and S. Seki, *Bull. Chem. Soc. Jpn*., **45**, 2398 (1972).
142 Q. Wang, Y. Yamamura, A. Takeuchi, K. Saito, M. Sorai, 15th International Conference on Chemical Thermodynamics, Porto, p. 4–8 (1998).
143 S. A. Roberts, D. R. Bloomquist, R. D. Willett, H. W. Dodgen, *J. Am. Chem. Soc*., **103**, 2603 (1981).
144 A. Nishimori and M. Sorai, *J. Phys. Chem. Solids*., **60**, 895 (1999).
145 S. Yamaki, Y. Fukuda, and K. Sone, *Chem. Lett*., **1982**, 269.
146 N. Hoshino, Y. Fukuda, K. Sone, K. Tanaka, and F. Marumo, *Bull. Chem. Soc. Jpn*., **62**, 1822 (1989).
147 H. Hara and M. Sorai, *J. Phys. Chem. Solids*, **56**, 223 (1995).
148 J. K. Burdett, *Adv. Inorg. Chem. Radiochem*., **21**, 113 (1978).
149 M. M. Andino, J. D. Curet, and M. M. Muir, *Acta Crystallogr.*, **B32**, 3185 (1976).
150 L. Grenthe, P. Paoletti, M. Sandström, and S. Glikberg, *Inorg. Chem*., **18**, 2687 (1979).
151 A. B. P. Lever, E. Montovani, and J. C. Donimi, *Inorg. Chem*., **10**, 2424 (1971).
152 J. R. Ferraro, L. J. Basile, L. R. Gtsvos-Ineguez, P. Paoletti, and L. Fabbrizzi, *Inorg. Chem*., **15**, 2342 (1976).
153 R. J. Pylkki, R. D. Willett, and H. W. Dodgen, *Inorg. Chem*., **23**, 594 (1984).
154 A. Nishimori, E. A. Schmitt, D. N. Hendrickson and M. Sorai, *J. Phys. Chem. Solids*, **55**, 99 (1994).
155 A. Nishimori, E. A. Schmitt, D. N. Hendrickson, and M. Sorai, *J. Coord. Chem*., **37**, 327 (1996).
156 A. Nishimori and M. Sorai, the 38th Annual Meeting on Coordination Chemistry, Tokushima, 3B16 (1988).

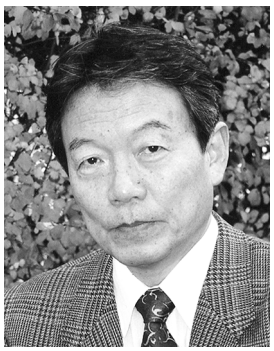

Michio Sorai was born in 1939 in Ryojun, then part of Japan. He received his B.Sc. degree in 1962, M.Sc. in 1964, and D.Sc. in 1968 from Osaka University. He was appointed as research associate of Department of Chemistry at Osaka University in 1964, and he was promoted to associate professor in 1981 and to full professor in 1987. Since 1993 he has been the director of the present (and also the former) Research Center for Molecular Thermodynamics at Osaka University. Since 1998 he has been appointed as associate member of the IUPAC I.2 Commission on thermodynamics, and for two years from October 1999 he served as the president of the Japan Society of Calorimetry and Thermal Analysis. He received the Hugh M. Huffman Memorial Award from the 56th Calorimetry Conference in August 2001. His research has been focused on molecular thermodynamic studies of phase transitions occurring in functional materials such as magnetic materials and liquid crystals, in particular phase transitions in which electrons are directly involved, such as spin crossover phenomena, intramolecular electron transfer in mixed-valence compounds, and thermochromic phenomena.